Ocean Science
Discussions

Open Access

EGU

Norwegian Sea net community production estimated from O_2 and prototype CO_2 optode measurements on a Seaglider

Luca Possenti[1], Ingunn Skjelvan[2], Dariia Atamanchuk[3], Anders Tengberg[4], Matthew P. Humphreys[5], Socratis Loucaides[6], Liam Fernand[7], Jan Kaiser[1]

[1]Centre for Ocean and Atmospheric Sciences, School of Environmental Sciences, University of East Anglia, Norwich, UK

[2]NORCE Norwegian Research Centre, Bjerknes Centre for Climate Research, Bergen, Norway

[3]Dalhousie University, Halifax, Canada

[4]University of Gothenburg, Sweden

[5]NIOZ Royal Netherlands Institute for Sea Research, Department of Ocean Systems (OCS), and Utrecht University, Texel, the Netherlands

[6]National Oceanography Centre, European Way, Southampton, SO14 3ZH, UK

[7]Centre for Environment, Fisheries and Aquaculture Sciences, Lowestoft, UK, NR33 0HT

Correspondence to: Luca Possenti (L.Possenti@uea.ac.uk)

Abstract. We report on a pilot study using a CO_2 optode deployed on a Seaglider in the Norwegian Sea for 8 months (March to October 2014). The optode measurements required drift- and lag-correction, and in situ calibration using discrete water samples collected in the vicinity. We found the optode signal correlated better with the concentration of CO_2, $c(CO_2)$, than with its partial pressure, $p(CO_2)$. Using the calibrated $c(CO_2)$ and a regional parameterisation of total alkalinity (A_T) as a function of temperature and salinity, we calculated total dissolved inorganic carbon concentrations, C_T, which had a standard deviation of 10 µmol kg^{-1} compared with direct C_T measurements. The glider was also equipped with an oxygen (O_2) optode. The O_2 optode was drift-corrected and calibrated using a $c(O_2)$ climatology for deep samples ($R^2 = 0.89$; RMSE = 0.009 µmol kg^{-1}). The calibrated data enabled the calculation of C_T- and oxygen-based net community production, $N(C_T)$ and $N(O_2)$. To derive N, C_T and O_2 inventory changes over time were combined with estimates of air-sea gas exchange and entrainment of deeper waters. Glider-based observations captured two periods of increased Chl a inventory in late spring (May) and a second one in summer (June). For the May period, we found $N(C_T) = (24\pm5)$ mmol m^{-2} d^{-1}, $N(O_2) = (61\pm14)$ mmol m^{-2} d^{-1} and an (uncalibrated) Chl a peak concentration of $c_{raw}(\text{Chl }a) = 3$ mg m^{-3}. During the June period, $c_{raw}(\text{Chl }a)$ increased to a summer maximum of 4 mg m^{-3}, which drove $N(C_T)$ to (64 ± 67) mmol m^{-2} d^{-1} and $N(O_2)$ to (166 ± 75) mmol m^{-2} d^{-1}. The high-resolution dataset allowed for quantification of the changes in N before, during and after the periods of increased Chl a inventory. After the May period, the remineralisation of the material produced during the period of increased Chl a inventory decreased $N(C_T)$ to (-80 ± 107) mmol m^{-2} d^{-1} and $N(O_2)$ to (-15 ± 27) mmol m^{-2} d^{-1}. The survey area was a source of O_2 and a sink of CO_2 for most of the summer. The deployment captured two different surface waters: the Norwegian Atlantic

34   Current (NwAC) and the Norwegian Coastal Current (NCC). The NCC was characterised by lower $c(O_2)$ and C_T

35   than the NwAC, as well as lower $N(O_2)$, $N(C_T)$ and $c_{raw}(Chl\ a)$. Our results show the potential of glider data to

36   simultaneously capture time and depth-resolved variability in C_T and O_2.

1 Introduction

37

38   Climate models project an increase in the atmospheric CO_2 mole fraction driven by anthropogenic emissions

39   from a preindustrial value of 280 µmol mol^{-1} (Neftel et al., 1982) to 538-936 µmol mol^{-1} by 2100 (Pachauri and

40   Reisinger, 2007). The ocean is known to be a major CO_2 sink (Sabine et al., 2004; Le Quéré et al., 2009; Sutton

41   et al., 2014), in fact has taken up approximately 25 % of this anthropogenic CO_2 with a rate of (2.5±0.6) Gt a^{-1}

42   (in C equivalents) (Friedlingstein et al., 2019). This uptake alters the carbonate system of seawater and is

43   causing a decrease in seawater pH, a process known as ocean acidification (Gattuso and Hansson, 2011). The

44   processes affecting the marine carbonate system include air-sea gas exchange, photosynthesis and respiration,

45   transport and vertical and horizontal mixing, and $CaCO_3$ formation and dissolution. For that reason, it is

46   important to develop precise, accurate and cost-effective tools to observe CO_2 variability and related processes

47   in the ocean. Provided that suitable sensors are available, autonomous ocean glider measurements may help

48   resolve these processes.

49   To quantify the marine carbonate system, four variables are commonly measured: total dissolved inorganic

50   carbon concentration (C_T), pH, total alkalinity (A_T) and the fugacity of CO_2 ($f(CO_2)$). At thermodynamic

51   equilibrium, knowledge of two of the four variables is sufficient to calculate the other two. Marine carbonate

52   system variables are primarily measured on research ships, commercial ships of opportunity, moorings, buoys

53   and floats (Hardman-Mountford et al., 2008; Monteiro et al., 2009; Takahashi et al., 2009; Olsen et al., 2016;

54   Bushinsky et al., 2019). Moorings equipped with submersible sensors often provide limited vertical and

55   horizontal, but good long-term temporal resolution (Hemsley, 2015). In contrast, ship-based surveys have higher

56   vertical and spatial resolution than moorings but limited repetition frequency because of the expense of ship

57   operations. Ocean gliders have the potential to replace some ship surveys because they are much cheaper to

58   operate and will increase our coastal and regional observational capacity. However, the slow glider speed of 1-2

59   km h^{-1} only allows a smaller spatial coverage than ship surveys and the sensors require careful calibration to

60   match the quality of data provided by ship-based sampling.

61   Carbonate system sensors suitable for autonomous deployment have been developed in the past decades, in

62   particular pH sensors (Martz et al., 2010; Rérolle et al., 2013; Seidel et al., 2008) and $p(CO_2)$ sensors (Goyet et

63   al., 1992; Degrandpre, 1993; Körtzinger et al., 1996; Bittig et al., 2012; Atamanchuk, 2013). One of these

Ocean Science
Discussions

64   sensors is the CO_2 optode (Atamanchuk et al., 2014) which has been successfully deployed to monitor an

65   artificial CO_2 leak on the Scottish west coast (Atamanchuk, et al., 2015b), on a cabled underwater observatory

66   (Atamanchuk, et al., 2015a), to measure lake metabolism (Peeters et al., 2016), for fish transportation (Thomas

67   et al., 2017) and on a moored profiler (Chu et al., 2020).

68   Oxygen and C_T can be used to calculate net community production (N), which is defined as the difference

69   between gross primary production (G) and community respiration (R). At steady-state, N is equal to the rate of

70   organic carbon export and transfer from the surface into the mesopelagic and deep waters (Lockwood et al.,

71   2012). N is derived by vertical integration to a specific depth, that is commonly defined relative to the mixed

72   layer depth (z_{mix}) or the bottom of the euphotic zone (Plant et al., 2016). A system is defined as autotrophic

73   when G is larger than R (i.e. N is positive) and as heterotrophic when R is larger than G (i.e. N is negative)

74   (Ducklow and Doney, 2013).

75   N can be quantified using bottle incubations, isotope methods (^{14}C, ^{15}N, ^{16}O/^{17}O/^{18}O) (Sharples et al., 2006;

76   Quay, et al, 2012; Seguro et al., 2019) or in situ biogeochemical budgets. Bottle incubations involve measuring

77   oxygen concentration driven by production and respiration in vitro under dark and light conditions.

78   Biogeochemical budgets combine O_2 and C_T inventory changes with estimates of air-sea gas exchange,

79   entrainment, advection and vertical mixing (Alkire et al., 2014; Binetti et al., 2020; Neuer et al., 2007).

80   The Norwegian Sea is a complex environment due to the interaction between the Atlantic Water (NwAC)

81   entering from the south-west, Arctic Water coming from north and the Norwegian Coastal Current (NCC)

82   flowing along the Norwegian coast (Nilsen and Falck, 2006). In particular, Atlantic Water enters the Norwegian

83   Sea through the Faroe-Shetland Channel and Iceland-Faroe Ridge (Hansen and Østerhus, 2000) with S between

84   35.1 and 35.3 and temperatures warmer than 6 ˚C (Swift, 1986). Furthermore, the NCC water mass differs from

85   the NwAC with a surface $S < 35$ (Saetre and Ljoen, 1972) and a seasonal θ signal (Nilsen and Falck, 2006).

86   Biological production in the Norwegian Sea varies during the year and can be divided into 5 periods (Rey,

87   2001): (1) winter with the smallest productivity and phytoplankton biomass; (2) a pre-bloom period; (3) the

88   spring bloom when productivity increases and phytoplankton biomass reaches the annual maximum; (4) a post-

89   bloom period with productivity mostly based on regenerated nutrients; (5) autumn with smaller blooms than in

90   summer. Previous estimates of $N(C_T)$ were based on discrete C_T samples (Falck and Anderson, 2005) or were

91   calculated from oxygen-based measurements and converted to C equivalents assuming Redfield stoichiometry

92   of production/respiration (Falck and Gade, 1999; Kivimäe, 2007; Skjelvan et al., 2001). Glider measurements

93   have been used to estimate N in other ocean regions (Nicholson et al., 2008; Alkire et al., 2014; Haskell et al.,

94   2019; Binetti et al., 2020); however, as far as we know, this is the first study of net community production in the

95   Norwegian Sea using a high-resolution glider dataset ($>10^6$ data points; 40 s time resolution) and the first

96   anywhere estimating N from a glider-mounted sensor directly measuring the marine carbonate system.

97   **2 Material and methods**

98   **2.1 Glider sampling**

99   Kongsberg Seaglider 564 was deployed in the Norwegian Sea on the 16 March 2014 at 63.00° N, 3.86° E and

100   recovered on the 30 October 2014 at 62.99° N, 3.89° E. The Seaglider was equipped with a prototype Aanderaa

101   4797 CO_2 optode, an Aanderaa 4330F oxygen optode (Tengberg et al., 2006), a Seabird CTD (GPCTD) and a

102   combined backscatter/chlorophyll *a* fluorescence sensor (Wetlabs Eco Puck BB2FLVMT). The mean time

103   needed by the sensor to reach a stable value for an in situ measurement (t) varied with depth (Table 1). On

104   average in the top 100 m the CTD performed an in situ measurement every 24 s, the O_2 optode every 49 s, the

105   CO_2 optode every 106 s and the fluorescence sensor every 62 s. The time to perform an in situ measurement

106   increased in depths between 100 to 500 m to 31 s for the CTD, 153 s for the O_2 optode and 233 s for the CO_2

107   optode. This measurement time reached its maximum at depths between 500 to 1000 m where was 42 s for the

108   CTD, 378 s for the O_2 optode and 381 d for the CO_2 optode.

109   **Table 1.** Average time needed by the Seabird CTD (GPCTD), Aanderaa 4330F oxygen optode, Aanderaa 4797
110   CO_2 optode and a combined backscatter/chlorophyll *a* fluorescence sensor (Wetlabs Eco Puck BB2FLVMT) to
111   perform an in situ measurement in the top 100 m, from 100 to 500 and from 500 to 1000 m.

Depth / m	t(CTD) / s	t(O_2) / s	t(CO_2) / s	t(Chl *a*) / s
0 – 100 m	24	49	106	62
100 – 500 m	31	153	233	-
500 – 1000 m	42	378	381	-

112

113   The deployment followed the Svinøy trench, from the open sea towards the Norwegian coast. The glider

114   covered a 536 km long transect 8 times (4 times in each direction) for a total of 703 dives (Figure 1).

115
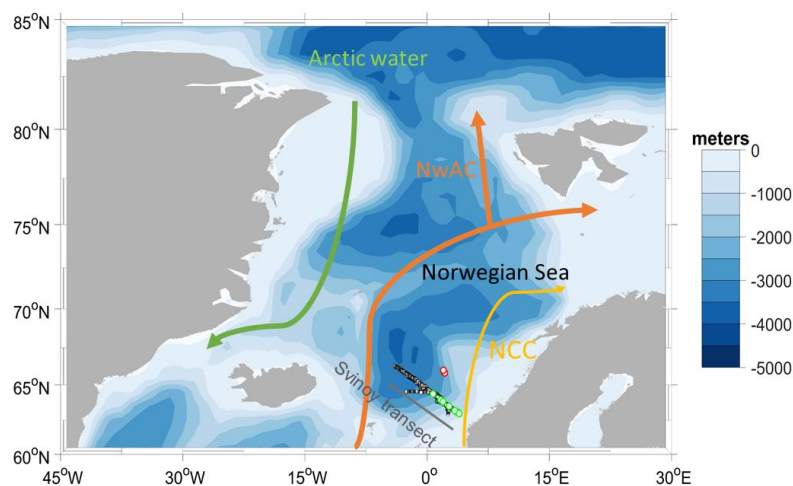
116
117 **Figure 1:** Map of the glider deployment and the main water masses. The black dots are the glider dives, the
118 green and the red dots are the water samples collected along the glider section and at OWSM, respectively. The
119 three main water masses (Skjelvan et al., 2008) are the Norwegian Coastal Current (yellow), the Norwegian
120 Atlantic Current (NwAC, orange) and Arctic Water (green).
121
122
123 **2.2 Discrete sampling**

124 During the glider deployment, 70 discrete water samples from various depths (5, 10, 20, 30, 50, 100, 300, 500

125 and 1000 m) were collected on 4 different cruises on the R/V Haakon Mosby along the southern half of the

126 glider transect on the 18 March, the 5 May, 6 and 14 June, and the 30 of October 2014. Samples for C_T and A_T

127 were collected from 10 L Niskin bottles following the standard operational procedure (SOP) 1 of Dickson et al.

128 (2007). The C_T and A_T samples were preserved with saturated $HgCl_2$ solution (final $HgCl_2$ concentration: 15 mg

129 dm^{-3}). Nutrient samples from the same Niskin bottles were preserved with chloroform. C_T and A_T were analysed

130 on-shore according to SOP 2 and 3b (Dickson et al., 2007) using a VINDTA 3D (Marianda) with a CM5011

131 coulometer (UIC instruments) and a VINDTA 3S (Marianda), respectively. Nutrients were analysed on-shore

132 using a an Alpkem Auto Analyzer. In addition, 43 water samples were collected at Ocean Weather Station M

133 (OWSM) on 5 different cruises on the 22 March on R/V Haakon Mosby, the 9 May on R/V G.O. Sars, the 14

134 June on R/V Haakon Mosby, the 2 August and the 13 November on R/V Johan Hjort from 10, 30, 50, 100, 200,

135 500, 800 and 1000 m depth. The OWSM samples were preserved and analysed for A_T and C_T similar to the

136 Svinøy samples. No phosphate and silicate samples were collected from OSWM. Temperature (θ) and salinity

137 (S) profiles were measured at each station using a SeaBird 911 plus CTD. pH and $f(CO_2)$ were calculated using

138 the MATLAB toolbox CO2SYS (Van Heuven et al., 2011), with the following constants: K_1 and K_2 carbonic

139 acid dissociation constants of Lueker et al. (2000), $K(HSO_4^-/SO_4^{2-})$ bisulfate dissociation constant of Dickson

140   (1990) and borate to chlorinity ratio of Lee et al. (2010). In the OWSM calculations, we used nutrients collected

141   from the Svinøy section at a time as close as possible to the OWSM sampling as input. In the case of the glider,

142   we derived a parameterisation to derive phosphate and silicate concentration as a function of the discrete sample

143   depth and time. This parameterisation had an uncertainty of 1.3 and 0.13 µmol kg^{-1}, for silicate and phosphate

144   concentrations, respectively.

145   **2.3 Oxygen optode calibration**

146   The last oxygen optode calibration before the deployment was performed in 2012 as a two-point calibration at

147   9.91 °C in air-saturated water and at 20.37 °C in anoxic Na_2SO_3 solution. Oxygen optodes are known to be

148   affected by drift (Bittig et al., 2015), which is worse for the fast-response foils used in the 4330F optode for

149   glider deployments. It has been suggested to calibrate and drift correct the optode using discrete samples or in-

150   air measurements (Nicholson and Feen, 2017). Unfortunately, no discrete samples were collected at the glider

151   deployment or recovery.

152   To overcome this problem, we used archived data to correct for oxygen optode drift. These archived

153   concentration data (designated $c_C(O_2)$) were collected at OWSM between 2001 and 2007 (downloaded from

154   ICES data base) and from the deployment region between 2000 and 2018 (extracted from GLODAPv2; Olsen et

155   al., 2016). To apply the correction, we used the oxygen samples corresponding to a potential density $\sigma_0 > 1028$

156   kg m^{-3} (corresponding to depths between 427 and 1000 m), because waters of these potential densities were

157   always well below the mixed layer and therefore subject to limited seasonal and interannual variability. The

158   salinity S of these samples varied from 34.88 to 34.96, with a mean of 34.90±0.01; θ varied from 0.45 to –0.76

159   °C, with a mean of (–0.15±0.36) °C.

160   Figure 2 shows that the glider oxygen concentration ($c_G(O_2)$) where $\sigma_0 > 1028$ kg m^{-3} was characterised by two

161   different water masses separated at a latitude of about 64° N. We used the samples collected north of 64° N to

162   derive the glider optode correction because this reflects the largest area covered by the glider. It was not possible

163   to use the southern region because it contained the archived samples from only 5 days. For each year-day with

164   archived samples, we calculated the median concentration of the glider and the archived samples. Figure 3

165   shows a plot of the ratio between $c_C(O_2)/c_G(O_2)$ against year-day and a linear fit, which is used to calibrate

166    $c_G(O_2)$ and correct for drift.
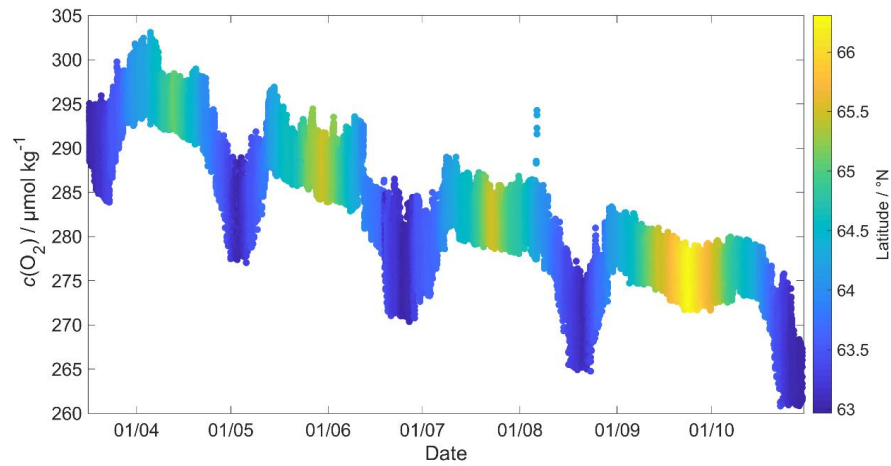
167
168 **Figure 2:** Glider oxygen concentration, $c_G(O_2)$, under $\sigma_0 = (1028\pm0.02)$ kg m^{-3} coloured by latitude.
169

170 No lag correction was applied because the O_2 optode had a fast response foil and showed no detectable lag (<10

171 s), based on a comparison between descent and ascent profiles.

172
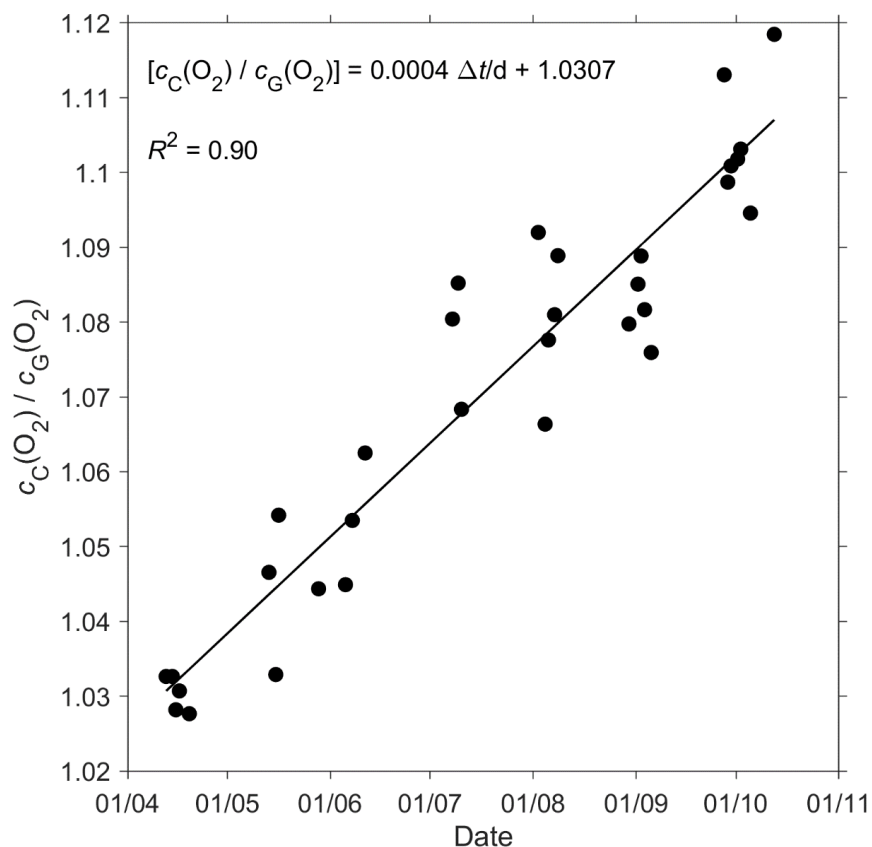
173
174 **Figure 3:**. The linear fit of the ratio between the daily median of the discrete oxygen samples ($c_C(O_2)$) and
175 glider oxygen data ($c_G(O_2)$) for $\sigma_0 > 1028$ kg m^{-3} was used to derive the $c_G(O_2)$ drift and initial offset at
176 deployment. The time interval Δt is calculated with respect to the deployment day of the 16th of March.
177

178 **2.4 CO$_2$ optode measurement principle**

179 The CO$_2$ optode consists of an optical and a temperature sensor incorporated into a pressure housing. The

180 optical sensor has a sensing foil comprising two fluorescence indicators (luminophores), of which one is

181 sensitive to pH changes and the other is not and thus used as a reference. The excitation and emission spectra of

182 the two fluorescence indicators overlap, but the reference indicator has a longer fluorescence lifetime than the

183 pH indicator. These two fluorescence lifetimes are combined using an approach known as Dual Lifetime

184 Referencing (DLR) (Klimant et al., 2001; von Bültzingslöwen et al., 2002). From the phase shift (φ), the partial

185 pressure of CO$_2$, $p(CO_2)$, is parameterised as an eight-degree polynomial (Atamanchuk et al., 2014):

186 $\log [p(CO_2)/\mu atm] = C_0 + C_1\,\varphi + \ldots + C_8\,\varphi^8$ (1)

187   where C_0 to C_8 are temperature-dependent coefficients.

188   The partial pressure of CO_2 is linked to the CO_2 concentration, $c(CO_2)$, and the fugacity of CO2, $f(CO_2)$, via the

189   following relationship:

190     $c(CO_2) = p(CO_2) / [1 - p(H_2O) / p] \, F(CO_2) = K_0(CO_2) \, f(CO_2)$ (2)

191   where $F(CO_2)$ is the solubility function (Weiss and Price, 1980), $p(H_2O)$ is the water vapour pressure, p is the

192   total gas tension (assumed to be near 1 atm) and $K_0(CO_2)$ is the solubility coefficient. F and K_0 vary according to

193   temperature and salinity.

2.5 CO_2 optode lag and drift correction

195   The CO_2 optode was fully functional between dives 31 (the 21 March 2014) and 400 (the 24 July 2014). After

196   dive 400, the CO_2 optode stopped sampling in the top 150 m. Figure 4 shows the outcome of each calibration

197   step described in this section (steps 1 and 2) and section 2.6 (step 3): 0) uncalibrated optode output (blue dots),

198   1) drift correction (red dots), 2) lag correction (green dots) and 3) calibration using discrete water samples

199   (black dots).
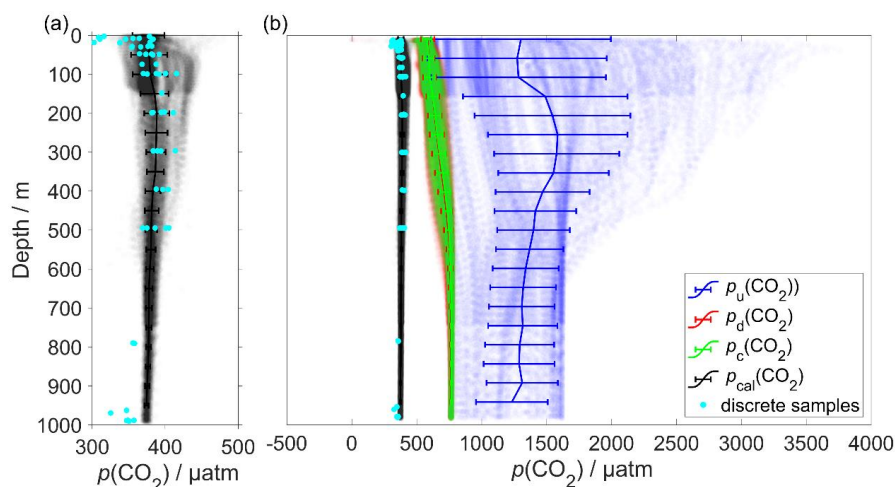
Figure 4: a) shows in black the calibrated $p(CO_2)$ ($p_{cal}(CO_2)$) and in azure the discrete samples b) $p(CO_2)$ versus depth where the vertical continuous lines are the mean every 50 m and the error bars represent the standard deviation. Blue colour shows $p_u(CO_2)$ without any correction; red shows $p_d(CO_2)$ corrected for drift, green represents $p_c(CO_2)$ corrected for drift and lag; black shows $p_{cal}(CO_2)$ calibrated against water samples (azure dots) collected during the deployment (section 2.6). $p_{cal}(CO_2)$ had a mean standard deviation of 22 µatm and a mean bias of 8.4 µatm compared with the discrete samples.

208   In order to correct for the drift occurring during the glider mission, we selected the CO_2 optode measurements in

209   water with $\sigma_0 > 1028$ kg m^{-3} (just as for O_2; section 2.3). We calculated the median of the raw optode phase shift

Ocean Science
Discussions

210   data ("CalPhase" φ_{cal}) for each Seaglider dive. Then, we calculated a drift coefficient (m_i) as the ratio between

211   the median φ_{cal} for a given dive divided by the median φ_{cal} of dive 31. Drift-corrected $\varphi_{cal,d}$ values were

212   calculated by dividing the raw φ_{cal} by the specific m_i for each dive.

213   The CO_2 optode was also affected by lag (Atamanchuk et al., 2014) caused by the slow response of the optode

214   to ambient $c(CO_2)$ changes in time and depth. The lag created a discrepancy between the depth profiles obtained

215   during glider ascents and descents. To correct for this lag we applied the method of Miloshevich et al. (2004),

216   which was previously used by Fiedler et al. (2013) and Atamanchuk et al. (2015b) to correct the lag of the

217   Contros HydroC CO_2 sensor (Fiedler et al., 2013; Saderne et al., 2013). This CO_2 sensor has a different

218   measurement principle (infrared absorption) than the CO_2 optode, but both rely on the diffusion of CO_2 through

219   a gas-permeable membrane.

220   To apply the lag correction, the sampling interval (Δt) needs to be sufficiently small compared to the sensor

221   response time (τ) and the ambient variability (Miloshevich, 2004). Before the lag correction, $\varphi_{cal,d}$ was

222   rLOWESS-smoothed to remove any outliers and "kinks" in the profile. The smoothing function applies a local

223   regression every 9 points using a weighted robust linear least-squares fit. Subsequently, τ was determined such

224   that the following lag-correction equation (Miloshevich, 2004) minimised the $\varphi_{cal,d}$ difference between each

225   glider ascent and the following descent:

226    $$p_c(CO_2, t_1) = \frac{p_d(CO_2, t_1) - p_d(CO_2, t_0)\ e^{-\Delta t/\tau}}{1 - e^{-\Delta t/\tau}}$$ (3)

227   where $p_d(CO_2, t_0)$ is the drift-corrected value measured by the optode at time t_0, $p_m(CO_2, t_1)$ is the measured value

228   at time t_1, Δt is the time between t_0 and t_1, τ is the response time, and $p_c(CO_2, t_1)$ is the lag-corrected value at t_1.

229   We calculated a τ value for each glider dive and used the median of t_0 (1384 s , 25th quartile: 1101 s; 75th

230   quartile: 1799 s) (Figure 5), which was larger than Δt (258 s) and therefore met the requirement to apply the

231   Miloshevich (2004) method. This lag correction decreased the average difference between the glider ascent and

232   descent from (71±30) µatm to (21±26) µatm.

Ocean Science
Discussions

Open Access

EGU

233
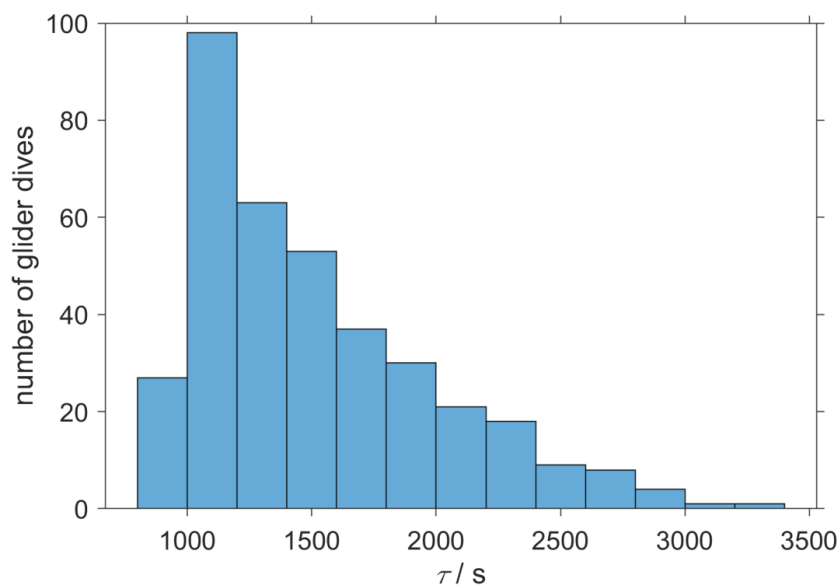
Figure 5: The histogram shows the distribution of the τ calculated from glider dive 31 to 400 to correct the CO_2 optode drift using the algorithm of Miloshevich (2004).

236

2.6 CO_2 optode calibration

238   The CO_2 optode output was calibrated using the discrete samples collected throughout the mission. Using the
239   discrete sample time and potential density σ_0, we selected the closest CO_2 optode output. Figure 6 shows a linear
240   regression between optode output and $c(CO_2)$ from the discrete samples ($c_{WS}(CO_2)$), which was used to calibrate
241   the optode output $p_c(CO_2)$ in terms of $c(CO_2)$. We used $c(CO_2)$ because it had a better correlation than $p(CO_2)$
242   ($R^2 = 0.77$ vs. $R^2 = 0.02$). The residual difference in $c(CO_2)$ between glider and water samples had a standard
243   deviation of 1.3 μmol kg^{-1}.

244

Ocean Science
Discussions
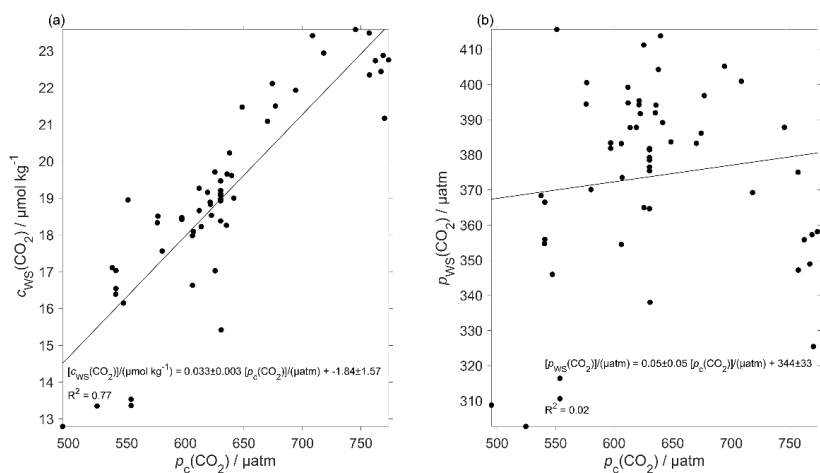
245 **Figure 6:** Calibration of the CO_2 optode using a) CO_2 concentration of the discrete samples ($c_{WS}(CO_2)$) against
246 the glider output with the linear regression line and b) CO_2 partial pressure of the discrete samples ($p_{WS}(CO_2)$)
247 against the glider output with the linear regression line.
248

249 **2.7 Regional algorithm to estimate A_T**

250 To calculate C_T, we used two variables: glider $c(CO_2)$ derived as described in section 2.6 and A_T derived using a

251 regional algorithm that uses the top 1000 m S and θ. The algorithm followed the approach of Lee et al. (2006)

252 and was derived using 663 water samples collected at OWSM from 2004 to 2014 and GLODAPv2 (Olsen et al.,

253 2016) data from 2000 in the deployment region. Discrete samples with $S < 33$ were removed because these

254 values were lower than the minimum S measured by the glider. The derived A_T parameterisation is:

255 $A_{T,reg} / (\mu mol\ kg^{-1}) = 2317.03 + 33.12\ (S–35) + 7.94\ (S–35)^2 + 0.96\ (\theta/°C–20) + 0.01\ (\theta/°C–20)^2$ (4)

256 The parameterisation has an uncertainty of 8.2 µmol kg^{-1} calculated as the standard deviation of the residual

257 difference between actual and parameterised A_T.

258 To test this parameterisation, we compared the predicted $A_{T,reg}$ values with discrete measurements ($A_{T,WS}$)

259 collected close in terms of time, potential density (σ_0) and distance to the glider transect ($n = 60$). These discrete

260 samples and the glider had the mean temperature and salinity differences of (0.17±0.68) °C and 0.03±0.013,

261 respectively. The mean difference between $A_{T,WS}$ and $A_{T,reg}$ was (2.1±6.5) µmol kg^{-1}.

262 This A_T parameterisation was used in CO2SYS (Van Heuven et al., 2011) to calculate C_T from $A_{T,reg}$ and the

263 calibrated $c(CO_2)$, $c_{G,cal}(CO_2)$. These calculated $C_{T,cal}$ values were compared with $C_{T,WS}$ of the same set of

264 discrete samples used to calibrate $c_{G,cal}(CO_2)$, the only difference being that instead of the actual total alkalinity

265 of the water sample ($A_{T,WS}$), we used $A_{T,reg}$. The mean difference between $C_{T,cal}$ and $C_{T,reg}$ was (1.5±10) µmol

266 kg^{-1}, with the non-zero bias and the standard deviation due to the uncertainties in the A_{Treg} parameterisation and

267 the $c_{G,cal}(CO_2)$ calibration.

268 **2.8 Quality control of other measurement variables**

269 The thermal lag of the glider conductivity sensor was corrected for (Gourcuff, 2014). Single-point outliers in

270 conductivity were removed and replaced by linear interpolation. The glider CTD salinity was affected by

271 presumed particulate matter stuck in the conductivity cell (Medeot et al., 2011) during dives 147, 234, 244, 251,

272 272, 279, 303, 320 and 397 and sensor malfunction caused a poor match between glider ascent and descent

273 during a dives 214, 215, 235 and 243. These dives were removed from the subsequent analysis.

Ocean Science
Discussions

274 Glider-reported chlorophyll concentrations, $c_{raw}(Chl\ a)$, were affected by photochemical quenching during the

275 daytime dives. To correct for quenching, we used the method of Hemsley et al. (2015) based on the nighttime

276 relationship between fluorescence and optical backscatter. This relationship was established in the top 60 meters

277 and the nighttime values were selected between sunset and sunrise. We calculated a linear fit between $c_{raw}(Chl$

278 $a)$ measured at night, $c_N(Chl\ a)$, and the backscatter signal measured at night (b_N). The slope and the intercept

279 were then used to correct daytime $c_D(Chl\ a)$. The glider-reported chlorophyll concentration has not been

280 calibrated against in situ samples and is not expected to be accurate, even after correction for quenching.

281 However, it should give an indication of the depth of the deep chlorophyll concentration maximum (z_{DCM}) and

282 the direction of chlorophyll concentration change (up/down). 8 day-means of $c_{raw}(Chl\ a)$ were compared with

283 satellite 8 day-composite chlorophyll concentration (Figure 7) from Ocean Colour CCI (https://esa-

284 oceancolour-cci.org/) and gave a mean difference of (0.12±0.08) mg m^{-3}.
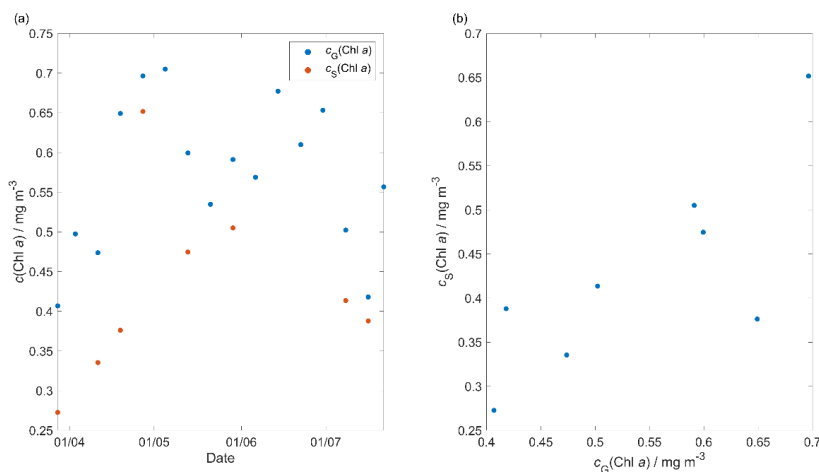
285

286 **Figure. 7:** comparison between the 8 days glider $c(Chl\ a)$ ($c_G(Chl\ a)$) mean and the 8 days satellite $c(Chl\ a)$
287 ($c_S(Chl\ a)$) download from Ocean Colour CCI (https://esa-oceancolour-cci.org/) where in a) $c_G(Chl\ a)$ in red
288 and $c_S(Chl\ a)$ in blue variability in time and in b) the direct comparison between $c_G(Chl\ a)$ and $c_S(Chl\ a)$.

289 **2.9 Calculation of oxygen-based net community production $N(O_2)$**

290 Calculating N from glider data is challenging because the glider continuously moves through different water

291 masses. In particular, during the deployment, the glider sampled two different water masses: the Norwegian

292 Coastal Current (NCC) and the Norwegian Atlantic Current (NwAC) (Nilsen and Falck, 2006). During the

293 summer, the winds drive the NCC away from the coast (Skjelvan et al., 2008), and in July and August the glider

294 measured S between 32 and 34 in the top 50 m. The two water masses were distinguished by different salinities;

295 the NwAC is saltier than the NCC (Nilsen and Falck, 2006; Swift, 1986). A threshold of $S = 35$ was used to

296   distinguish between NCC and NwAC. We further subdivided the transect by binning the data into 0.1° latitude

297   intervals to derive O_2 concentration changes between transects.

298   We calculated $N(O_2)$ from the oxygen inventory changes ($\frac{\Delta I(O_2)}{\Delta t}$) corrected for air-sea exchange $\Phi(O_2)$

299   normalised to z_{mix} when z_{mix} was deeper than the integration depth of $z_{lim} = 45$ m and entrainment $E(O_2)$:

300    $$N(O_2) = \frac{\Delta I(O_2)}{\Delta t} + \Phi(O_2)\frac{\min(z_{lim},z_{mix})}{z_{mix}} - E(O_2) \qquad (5)$$

301   The inventory changes were calculated as the difference between transects of the integrated $c(O_2)$ in the top 45

302   m. A constant integration depth of 45 m was chosen to capture the deepest extent of the deep chlorophyll

303   maximum (z_{DCM}) found during the deployment, which likely represents the lower bound for the euphotic zone.

304   The inventory changes were calculated using the following equation:

305    $$\frac{\Delta I(O_2)}{\Delta t} = \frac{\int_0^{45\,m} C_{n+1}dz - \int_0^{45\,m} C_n dz}{t_{n+1} - t_n} \qquad (6)$$

306   where n is the transect number, t is the year-day and C is $c(O_2)$.

307   The air-sea flux of oxygen, $\Phi(O_2)$ was calculated for each glider dive using the median $c(O_2)$, θ and S in the top

308   10 m. We followed the method of Woolf and Thorpe (1991) that includes the effect of bubble equilibrium

309   supersaturation in the calculations:

310    $$\Phi(O_2) = k_w(O_2) \{(c(O_2) - [1 + \Delta_{bub}(O_2)]c_{sat}(O_2)\} \qquad (7)$$

311   where $k_w(O_2)$ is the gas transfer coefficient, $\Delta_{bub}(O_2)$ is the increase of equilibrium saturation due to bubble

312   injection and $c_{sat}(O_2)$ is the oxygen saturation. $c_{sat}(O_2)$ was calculated from S and θ using the solubility

313   coefficients of Benson and Krause Jr (1984), as fitted by Garcia and Gordon (1992). $\Delta_{bub}(O_2)$ was calculated

314   from the following equation:

315    $$\Delta_{bub}(O_2) = 0.01 \left(\frac{U}{U_0}\right)^2 \qquad (8)$$

316   where U is 10 m-wind speed with 6 hours resolution (ECMWF ERA InterimDaily,

317   https://apps.ecmwf.int/datasets/data/interim-full-daily/levtype=sfc/) and U_0 represents the wind speed

318   when the oxygen concentration is 1 % supersaturated and has a value of 9 m s^{-1} (Woolf and Thorpe, 1991). U

319   has a spatial resolution of 0.75° latitude and 0.75° longitude and was interpolated to the glider position at the

320   beginning of the dive.

321   The transfer velocity $k_w(O_2)$ was calculated based on Wanninkhof (2014):

322 $$\frac{k_{\mathrm{w}}(\mathrm{O}_2)}{\mathrm{cm\,h}^{-1}} = 0.251 \left(\frac{Sc(\mathrm{O}_2)}{660}\right)^{-0.5} \left(\frac{U}{\mathrm{m\,s}^{-1}}\right)^2 \tag{9}$$

323 The Schmidt number, $Sc(\mathrm{O}_2)$, was calculated using the parameterisation of Wanninkhof (2014).

324 The entrainment flux, $E(\mathrm{O}_2)$, was calculated as the oxygen flux when the mixed layer depth deepens in time and

325 is greater than z_{lim} at time t_2:

326 $$E(\mathrm{O}_2) = \frac{I(\mathrm{O}_2,t_1,z_{\mathrm{mix}}(t_2))\frac{z_{\mathrm{lim}}}{z_{\mathrm{mix}(t_2)}} - I(\mathrm{O}_2,t_1,z_{\mathrm{lim}})}{t_2 - t_1} \tag{10}$$

327 where $t_2 - t_1$ represents the change in time, z_{mix} is the mixed layer depth, $I(\mathrm{O}_2,t_1,z_{\mathrm{mix}}(t_2))$, is the expected

328 inventory that would result from a mixed layer deepening to $z_{\mathrm{mix}}(t_2)$ between t_2 and t_1, and $I(\mathrm{O}_2,t_1,z_{\mathrm{lim}})$ is the

329 original inventory at t_1.

330 Then, we calculated $N(\mathrm{O}_2)$ with $\frac{\Delta I(\mathrm{O}_2)}{\Delta t}$ corrected for $\Phi(\mathrm{O}_2)$ and $E(\mathrm{O}_2)$ using equation 5.

331 **2.10 Calculation of dissolved inorganic carbon-based net community production, $N(C_{\mathrm{T}}$**

332 $N(C_{\mathrm{T}})$ was calculated from the C_{T} inventory changes $\frac{\Delta I(C_{\mathrm{T}})}{\Delta t}$, air-sea flux of CO_2, $\Phi F(CO_2)$, and entrainment

333 $E(C_{\mathrm{T}})$:

334 $$N(C_{\mathrm{T}}) = -\frac{\Delta I(C_{\mathrm{T}})}{\Delta t} - \Phi(CO_2)\frac{\min(z_{\mathrm{lim}},z_{\mathrm{mix}})}{z_{\mathrm{mix}}} + E(C_{\mathrm{T}}) \tag{11}$$

335 Firstly, $\Phi(CO_2)$ was calculated using the 10 m wind speed with 6 hours' resolution downloaded from ECMWF

336 ERA Interim Daily. As for oxygen, we selected the closest wind speed data point at the beginning of each glider

337 dive. We used the monthly mean atmospheric CO_2 dry mole fraction ($x(CO_2)$) downloaded from the Greenhouse

338 Gases Reference Network Site from (https://www.esrl.noaa.gov/gmd/ccgg/ggrn.php) the closest site to the

339 deployment at Mace Head, County Galway, Ireland (Dlugokencky et al., 2015). Using $x(CO_2)$ we calculated the

340 air-saturation concentration $c_{\mathrm{atm}}(CO_2)$:

341 $$c_{\mathrm{atm}}(CO_2) = x(CO_2)\, p_{\mathrm{baro}}\, F(CO_2) \tag{12}$$

342 where p_{baro} is the mean sea level pressure and $F(CO_2)$ is the CO_2 solubility function calculated from surface θ

343 and S (Weiss and Price, 1980).

344 The seawater $c(CO_2)$ at the surface was calculated using the median in the top 10 meters between the glider

345 ascent and descent of the following dive $c(CO_2)$. From this, $\Phi(CO_2)$ was calculated:

346 $$\Phi(CO_2) = k(CO_2)\,[c(CO_2) - c_{\mathrm{atm}}(CO_2)]. \tag{13}$$

347    $k(CO_2)$ was calculated using the parameterisation of Wanninkhof (2014):

348    $\dfrac{k(O_2)}{cm\,h^{-1}} = 0.251 \left(\dfrac{Sc(CO_2)}{660}\right)^{-0.5} \left(\dfrac{U}{m\,s^{-1}}\right)^2$ (14)

349    $Sc(CO_2)$ is the dimensionless Schmidt number at the seawater temperature (Wanninkhof, 2014).

350   The inventory changes were calculated in the top 45 m with the following equation:

351    $\dfrac{\Delta I(C)}{\Delta t} = \dfrac{\int_0^{45\,m} c_{n+1}dz - \int_0^{45\,m} c_n dz}{t_{n+1} - t_n}$ (15)

352   The entrainment flux, $E(C_T)$ was calculated as the oxygen flux when the mixed layer depth deepens in time and

353   is greater than z_{lim} at time t_2:

354    $E(C_T) = \dfrac{I(C, t_1, z_{mix}(t_2))\dfrac{z_{lim}}{z_{mix}(t_2)} - I(C, t_1, z_{lim})}{t_2 - t_1}$ (16)

355   The uncertainties in $N(C_T)$ and $N(O_2)$ were evaluated with a Monte-Carlo approach. The uncertainties of the

356   input variables are shown in Table 2; we repeated the analysis 1000 times. The total uncertainty in N was

357   calculated as the standard deviation of the 1000 Monte-Carlo simulations.

358   **Table 2.** Uncertainty associated with $N(C_T)$ and $N(O_2)$ input variables calculated by a Monte Carlo approach

Variable	Error	Reference/Method
C_T	10 µmol kg⁻¹	Standard deviation vs the water samples.
S	0.01	Standard deviation of glider salinities for $\sigma_0 > 1028$ kg m⁻³ and latitude $> 64°$ N
θ	0.3 °C	Standard deviation of glider temperature for $\sigma_0 > 1028$ kg m⁻³ and latitude $> 64°$ N
$c_{atm}(CO_2)$	1.5 µmol kg⁻¹	Standard deviation of $c_{atm}(CO_2)$
$c(CO_2)$	1.3 µmol kg⁻¹	Error is the standard deviation vs water samples.
$k(CO_2)$	20 %	(Wanninkhof, 2014)
z_{mix}	9 m	Standard deviation compared with z_{mix} based on thresholds $\Delta T = 0.1$ °C (Sprintall and Roemmich, 1999), 0.2 °C (Thompson, 1976) and 0.8 °C (Kara et al., 2000).
z_{mix} latitude	0.32 m	Standard deviation compared with z_{mix} based on thresholds $\Delta T = 0.1$ °C (Sprintall and Roemmich, 1999), 0.2 °C (Thompson, 1976) and 0.8 °C (Kara et al., 2000).
$c_G(O_2)$	2.4 µmol kg⁻¹	Standard deviation of glider oxygen concentrations for $\sigma_0 > 1028$ kg m⁻³ and latitude $> 64°$ N

359
360

361   **3 Results**

362   The uncorrected temperature θ, salinity S, $c(O_2)$, $p(CO_2)$ and $c_{raw}(Chl\ a)$ presented in Figure 8 were analysed to

363   dive 400 dive(24 July 2014) because after the CO_2 optode stopped sampling in the first 150 m (Figure 8d). The

364   rawdata $c(O_2)$ data was calibrated and drift corrected and $c(CO_2)$ was drift, lag and recalibrated and then used to

365   quantify the temporal and spatial changes in N and Φ together with the quenching corrected $c_{\mathrm{raw}}(\mathrm{Chl}\ a)$ to

366   evaluate the net community production changes.
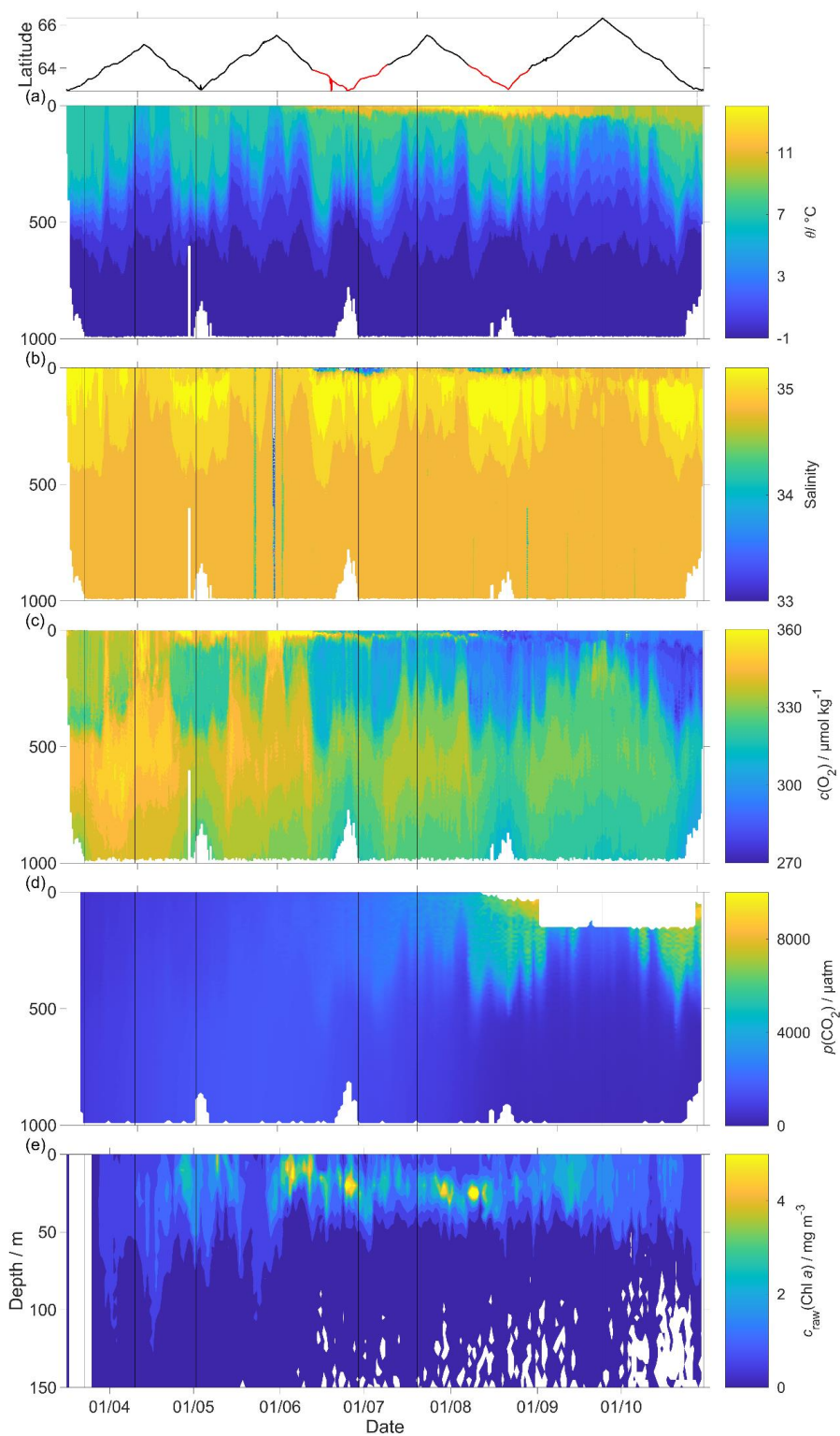
368
369 **Figure 8:** Raw glider data for all 703 dives with latitude of the glider trajectory at the top (black: NwAC; red:
370 NCC, separated by a S of 35). a) temperature θ, b) salinity S, c) oxygen concentration $c(O_2)$, d) uncorrected CO_2
371 optode output $p_u(CO_2)$ and e) chlorophyll a concentration $c_{raw}(Chl\ a)$. The white space means that the sensors
372 did not measure any data.
373
374 **3.1 O_2 optode calibration**

375 The uncorrected $c(O_2)$ continually decreased (Figure 8c). The ratio $c_C(O_2)/c_G(O_2)$ and against year-day used for

376 the drift correction had a good correlation with time ($R^2 = 0.90$), showing a continuous increase of 0.0004 d^{-1}

377 (Figure 3), equivalent to a decrease in the measured glider O_2 concentration of 0.11 µmol kg^{-1} d^{-1}. It was

378 possible to apply the correction because $c_C(O_2)$ had low temporal variability. The discrete oxygen samples from

379 OWSM and GLODAPv2 had a mean of (304.6±3.1) µmol kg^{-1}, varying from 294 to 315 µmol kg^{-1}. The drift

380 correction reduced the variability of $c_G(O_2)$ in the selected potential density range from a standard deviation of

381 7.3 µmol kg^{-1} to a standard deviation of 2.4 µmol kg^{-1} (Figure 9).

382
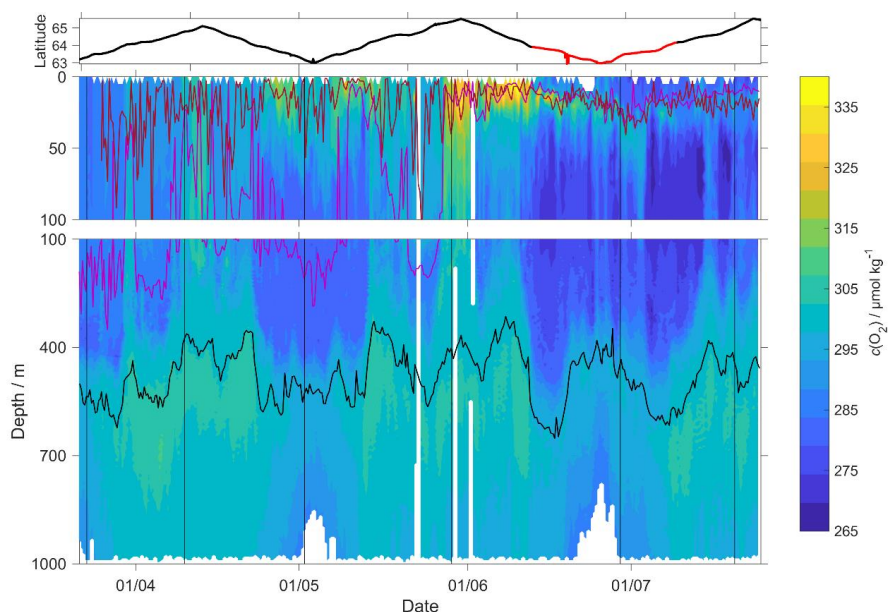
383
384 **Figure 9:** $c(O_2)$ contour plot with z_{DCM} (red line) and the z_{mix} (pink line) calculated using a threshold criterion of
385 $\Delta\theta = 0.5\ °C$ to median θ of the top 5 m of the glider profile (Obata et al., 1996; United States. National
386 Environmental Satellite and Information Service, Monterey and Levitus, 1997; Fo*ltz* et al., 2003), in black $\sigma_0 =$
387 1028 kg m^{-3} and at the top the latitude trajectory of the glider in black NwAC and in red NCC.
388

389 **3.2 CO_2 optode calibration**

390 Following drift, lag and scale corrections, glider fugacity $f_G(CO_2)$ derived from Eq. 2 had a mean difference of

391 (8±22) µatm to the discrete samples ($n = 55$; not shown) and C_T had a standard deviation of 10 µmol kg^{-1} and a

392 mean difference of 1.5 µmol kg^{-1} (Figure 10). $p(CO_2)$ and $f(CO_2)$ are almost the same numbers, specifically

393 $f(CO_2)$ takes into account of the non-ideal nature of the gas phase. The optode was able to capture the temporal

394 and spatial variability showing that NCC had a lower concentration of C_T than NwAC. Restricting the discrete

395 samples $f(CO_2)$ to the top 10 m only gave a mean difference of (21±21) µatm ($n = 8$). We also compared glider

396 $f_G(CO_2)$ with SOCAT $f(CO_2)$ (Bakker et al., 2016) data in the region during the deployment (Figure 11). Until

397 the beginning of June, there was general agreement between $f_G(CO_2)$ and $f_{SOCAT}(CO_2)$. Afterwards, $f_G(CO_2)$

398 varied between 326 and 434 µatm while $f_{SOCAT}(CO_2)$ varied between 259 and 354 µatm (Figure 11).

399 Our results are in agreement with Jeansson et al. (2011) that found the surface NCC was the region with the

400 lowest C_T values (2083 µmol kg^{-1}) in the Norwegian Sea. This was confirmed during our deployment because

401 C_T was (2100±18) µmol kg^{-1} in the NCC region and (2150±23) µmol kg^{-1} in the NwAC region (Figure 10) and

402 $c(O_2)$ was >300 µmol kg^{-1} in the NwAC and < 280 µmol kg^{-1} in the NCC.
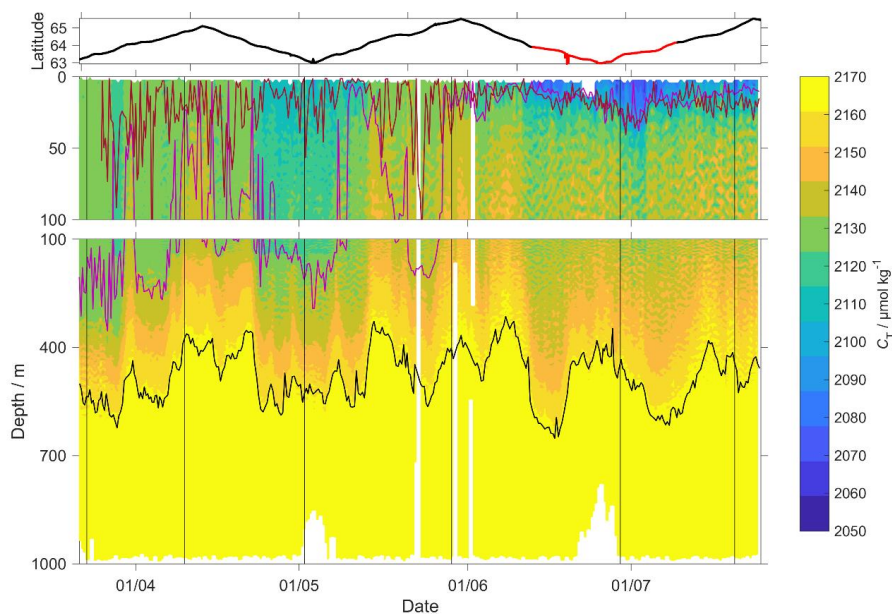
403
404 **Figure 10:** C_T contour plot with z_{DCM} (red line) and the z_{mix} (pink line) calculated using a threshold criterion of
405 $\Delta\theta = 0.5$ °C to median θ of the top 5 m of the glider profile (Obata et al., 1996; United States. National
406 Environmental Satellite and Information Service, Monterey and Levitus, 1997; Fo*ltz* et al., 2003), in black $\sigma_0 =$
407 1028 kg m^{-3} and at the top the latitude trajectory of the glider in black NwAC and in red NCC.
408
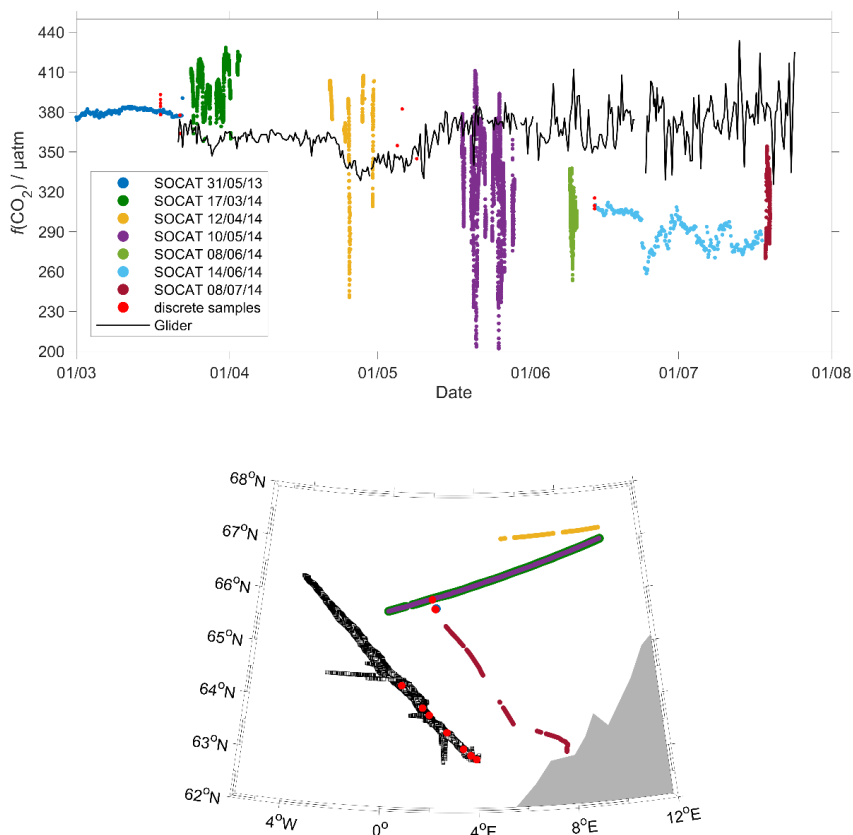
Figure 11: The plot represents the surface $f(CO_2)$ from 2014 SOCAT and from the glider. The black dots are the median of the glider $f(CO_2)$ in the top 10 meters calculated using the ascent of the single dive and the descent of the next dive. The red dots are the water samples collected during the deployment and the remaining dots are from the SOCAT cruises in the area during the deployment. On the bottom there is the map of the glider and SOCAT data positions.

3.3 Air-sea exchange

The surface water was supersaturated with oxygen all summer (Figure 12). From May this supersaturation drove

a continuous O_2 flux from the sea to the atmosphere. However, the flux varied throughout the deployment

having a median of 21 mmol m^{-2} d^{-1} (5th centile: -16 mmol m^{-2} d^{-1}; 95th centile: 102 mmol m^{-2} d^{-1}). Prior to the

spring period of increased Chl a inventory, the supersaturation varied between 0 to 10 µmol kg^{-1}. $\Phi(O_2)$ had a

median of -0.2 mmol m^{-2} d^{-1} (5th centile: -57 mmol m^{-2} d^{-1}; 95th centile: 12 mmol m^{-2} d^{-1}). Then, during the

spring period of increased Chl a inventory, the surface concentration increased by over 35 µmol kg^{-1}, causing a

peak in $\Phi(O_2)$ of 104 mmol m^{-2} d^{-1}. A second period of increased Chl a inventory was encountered in June and

424   had a larger $\Phi(O_2)$ up to 168 mmol m^{-2} d^{-1}, driven by supersaturation of 68 μmol kg^{-1}. These larger fluxes during

425   the second period of increased Chl a inventory were associated by an increase of c_{raw}(Chl a) from 2.5 mg m^{-3} to

426   the summer maximum of 4.0 mg m^{-3}. However, prior to the spring period of increased Chl a inventory, $\Phi(O_2)$

427   showed a few days of influx into seawater caused by a decrease of θ from 7.6 °C to 5.9 °C that increased

428    $c_{sat}(O_2)$. The influx at the beginning of the deployment is partly due to the $\Delta_{bub}(O_2)$ correction that increased [1+

429    $\Delta_{bub}(O_2)]c_{sat}(O_2)$ to values larger than $c(O_2)$ for $U > 10$ m s^{-1}.

430   The CO_2 flux from March to July was always from the air to the sea (Figure 13), with a median of -2.0 mmol m^{-}

431   ^{2} d^{-1} (5th centile: -11 mmol m^{-2} d^{-1}; 95th centile: 0.24 mmol m^{-2} d^{-1}). An opposite flux direction is expected for

432    $\Phi(O_2)$ and $\Phi(CO_2)$ during the productive season when net community production is the main driver of

433   concentration changes. After the summer period of increased Chl a inventory, the flux had a median of -0.32

434   mmol m^{-2} d^{-1} (5th centile: –2.4 mmol m^{-2} d^{-1}; 95th centile: 1.1 mmol m^{-2} d^{-1}). Positive fluxes (from water to air)

435   are in disagreement with previous studies that classified the Norwegian Sea as a CO_2 sink (Skjelvan et al., 2005;

436   Takahashi et al., 2002). Calculating $\Phi(CO_2)$ from the discrete samples from the 18 March to the 14 June (n =

437   13) the flux varied from 0.1 to -13 mmol m^{-2} d^{-1} with just one positive $\Phi(CO_2)$ in March.

Ocean Science
Discussions
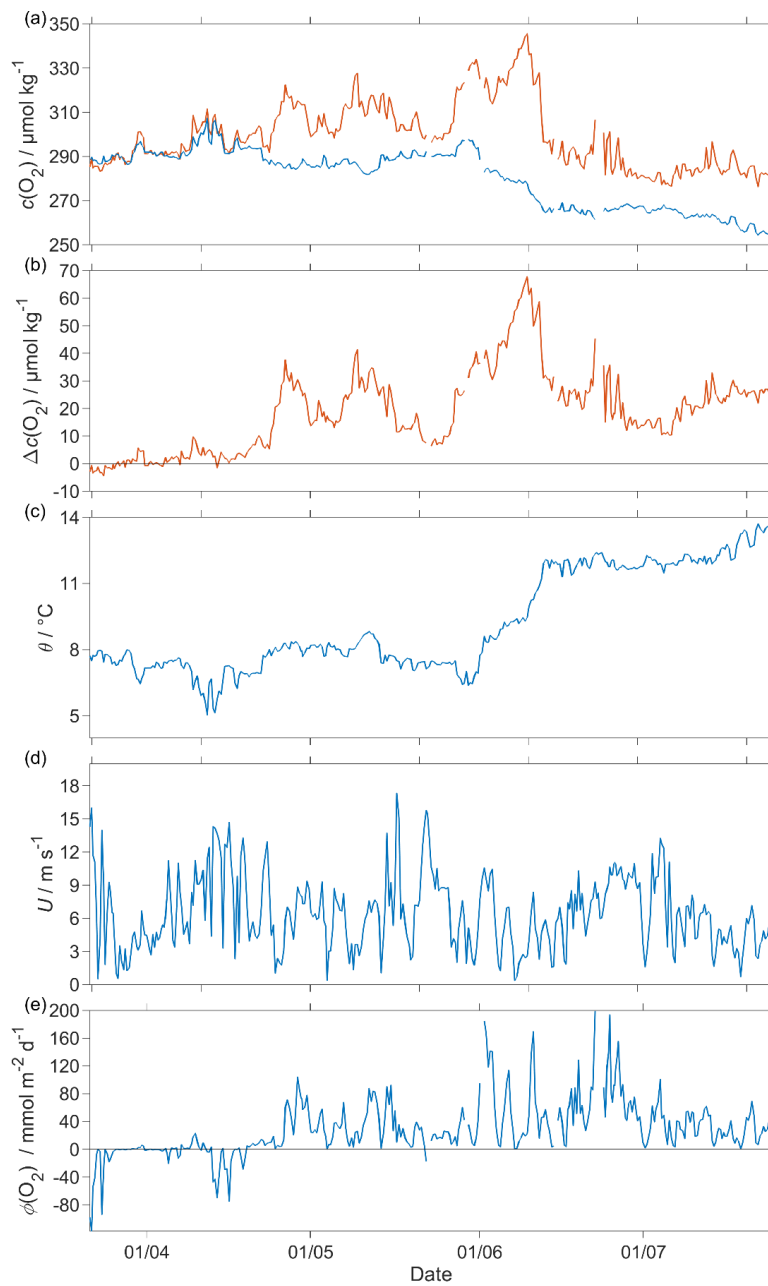
Figure 12: a) shows in blue $c_{sat}(O_2)$ and in red $c(O_2)$, b) the difference between $c(O_2)$ and $c_{sat}(O_2)$ ($\Delta c(O_2)$), c) the surface θ, d) 10 metre wind speed (U) and e) oxygen air-sea flux $\Phi(O_2)$ from sea to air for each glider dive. Flux from sea to air is positive while that from air to sea is negative.
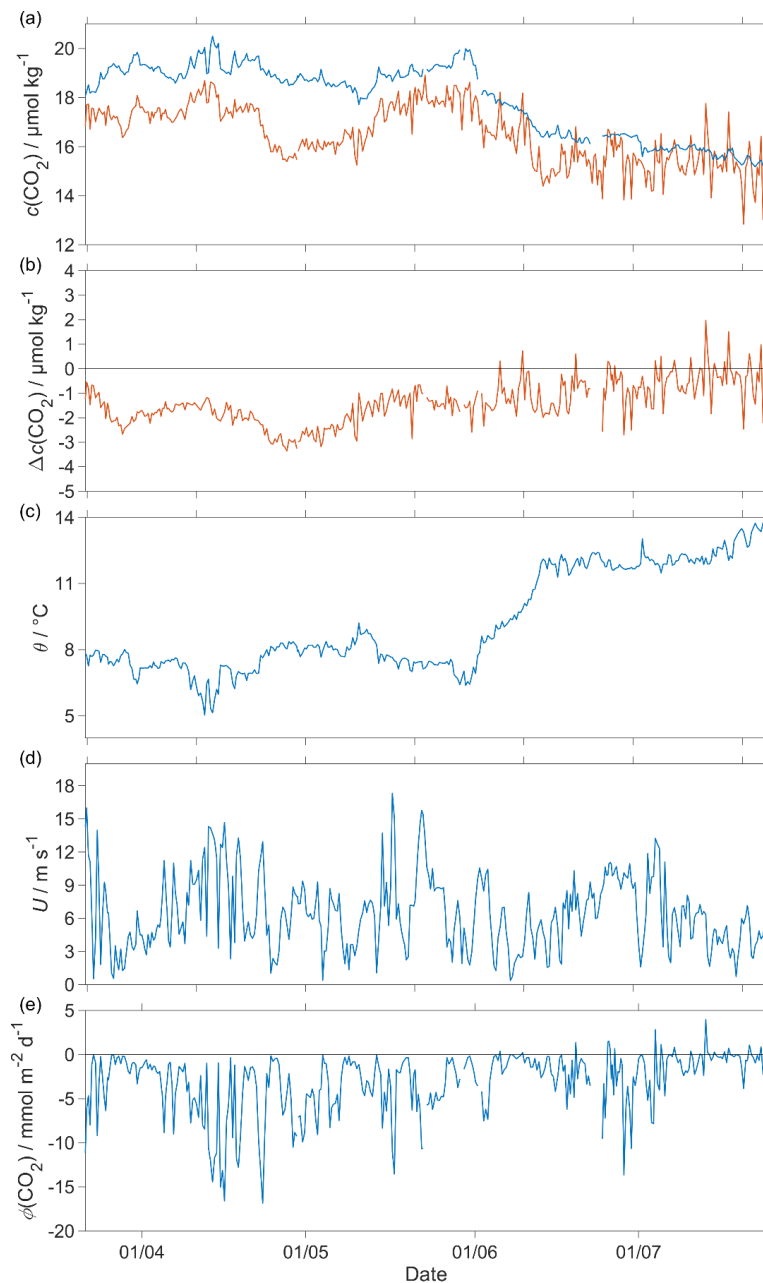
444
445
446 **Figure 13:** a) shows in blue $c_{sat}(CO_2)$ and in red $c(CO_2)$, b) the difference between $c(CO_2)$ and $c_{sat}(CO_2)$
447 ($\Delta c(CO_2)$), c) the surface θ, d) 10 metre wind speed (U)) and e) CO_2 air-sea flux $\Phi(CO_2)$ from sea to air for
448 each glider dive. Flux from sea to air is positive while that from air to sea is negative.
449

Ocean Science
Discussions

3.4 $N(O_2)$

450

451 We calculated $N(O_2)$ and $N(C_T)$ using an integration depth of z_{lim} = 45 m because the mean deep chlorophyll

452 maximum (DCM) depth was z_{DCM} = (20±18 m) (Figure 9). For comparison, the mixed layer depth was deeper

453 and varied more strongly and had a mean value of z_{mix} = (73±74) m, using a threshold criterion of $\Delta\theta = 0.5$ °C to

454 the median θ value of the top 5 m of the glider profile (Obata et al., 1996; United States. National

455 Environmental Satellite and Information Service, Monterey and Levitus, 1997; Foltz et al., 2003).

456 The two Ns were calculated as the difference in inventory changes between two transects when the glider was in

457 the same water mass. For that reason, Figures 14-16 starts from the second glider transect and in the second part

458 of no Ns values were calculated because the glider started the first transect in NCC.

459 During the deployment, we sampled two periods of increased Chl a inventory, the first one in May and a second

460 one in June. The Chloropyll a inventory ($I_{raw,z_{lim}}(Chl\,a)$) was calculated integrating $c_{raw}(Chl\,a)$ to z_{lim} The

461 fluorometer was not calibrated for that reason to remove any outliers we used a five points moving mean of

462 $I_{raw,z_{lim}}(Chl\,a)$.

463

465

Ocean Science
Discussions

Open Access

EGU
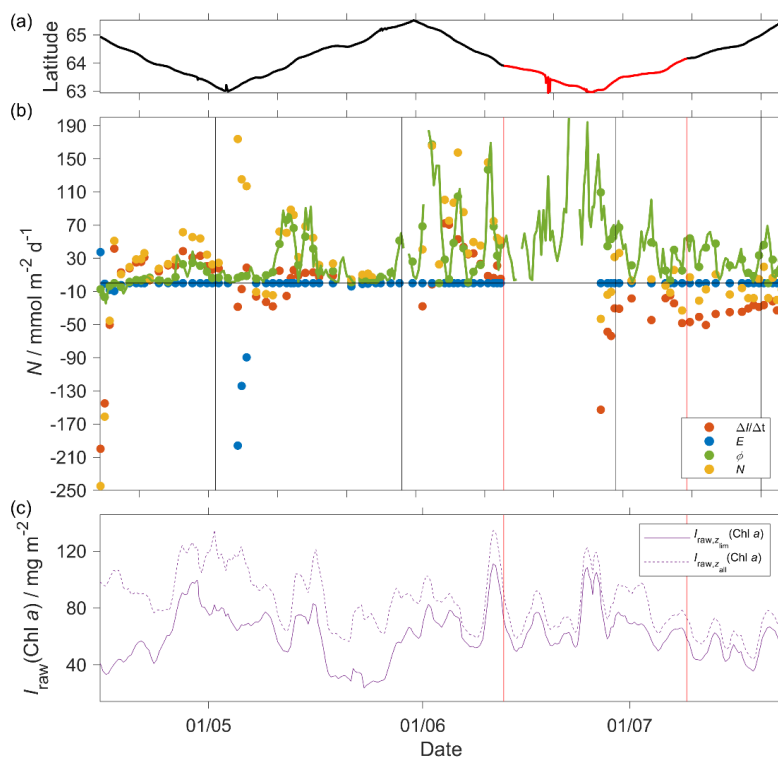
466 **Figure 14:** a) The trajectory in latitude of the glider where NwAC and NCC are in black and red, respectively .
467 b) Each component of the $N(O_2)$ calculation: in red $\frac{\Delta I(O_2)}{\Delta t}$, $E(O_2)$ in blue, $\Phi(O_2)$ in green dots and the green line
468 is $\Phi(O_2)$ continuous timeseries and in yellow $N(O_2) = \frac{\Delta I(O_2)}{\Delta t} + \Phi(O_2)\frac{\min(z_{lim}, z_{mix})}{z_{mix}} - E(O_2)$ c) the violet
469 continuous line is the c_{raw}(Chl a) inventory in the top 45 m, z_{lim}, $(I_{raw,z_{lim}}$(Chl a)) and the dotted line in all the
470 water columun, z_{all}, $(I_{raw,z_{all}}$(Chl a)). The black vertical lines represent each glider transect and between the two
471 vertical red lines the glider was in NCC.
472

473 During the summer $I_{raw,z_{lim}}$(Chl a) increased to 110 mg m^{-2}, which caused a sharp increase of $N(O_2)$ to

474 (166±75) mmol m^{-2} d^{-1}. However, we were not able to see the end of this productive period because the glider

475 moved into NCC. The passage of the glider from NwAC to NCC accompanied by a drop of surface $c(O_2)$ from

476 330 to 280 µmol kg^{-1} (Figure 9) that resulted in lower $\Phi(O_2)$ and $N(O_2)$ values (Figure 14).

477 At the beginning of May, $I_{raw,z_{lim}}$(Chl a) increased to 97 mg m^{-2} and $N(O_2) = $ (61±14) mmol m^{-2} d^{-1}. After this

478 period, $I_{raw,z_{lim}}$(Chl a) decreased to 49 mg m^{-2} and $N(O_2) = $ (-15±27) mmol m^{-2} d^{-1}. However, a deepening of

479 z_{mix} from 123 m to 206 m caused a spike in the entrainment flux $E(O_2)$ of 190 mmol m^{-2} d^{-1} that drove the

480 maximum $N(O_2)$ to (174±72) mmol m^{-2} d^{-1}.

481 Using the mean of $N(O_2)$ considering together NCC and NwAC and assuming an $N(O_2) = 0$ in the rest of the

482 year lead to an annual value of 10 mol m^{-2} a^{-1} (Table 3) discussed in section 4.3.

483 **Table 3.** N estimates in the Norwegian Sea
484

Study	$N(C_T)$ / mol m^{-2} a^{-1}	$N(O_2)$ / mol m^{-2} a^{-1}	z_{lim} / m	Variables used to derive N
(Falck and Anderson, 2005)	3.4	—	100	$c(NO_3^-)$, $c(PO_4^{3-})$, C_T
(Skjelvan et al., 2001)	2.0	2.6	300	$c(O_2)$, $c(PO_4^{3-})$
(Kivimäe, 2007)	8.6	11	z_{mix} until 100 m	$c(O_2)$
(Falck and Gade, 1999)	3.0	3.9	30	$c(O_2)$
This study	3.3	10	45	$c(O_2)$, C_T

485

486 **3.5 $N(C_T)$**

487 Before the spring period of increased Chl a inventory, $N(C_T)$ was (-15±14) mmol m^{-2} d^{-1} and increased to (23±5)

488 mmol m^{-2} d^{-1} during the period of increased Chl a inventory (Figure 15). Later during the summer high Chl a

489 period $N(C_T)$ had its summer maximum in NwAC at (64±67) mmol m^{-2} d^{-1}. The first transect in NCC was

490 characterised by an increase of $I_{raw,z_{lim}}$(Chl a) on the 11 June to 110 mg m^{-2} and $N(C_T)$ to (75±58) mmol m^{-2} d^{-}

491 ^{1}. Later, on the 4 July $N(C_T)$ decreased to (-14±22) mmol m^{-2} d^{-1} when $I_{raw,z_{lim}}$(Chl a) dropped to 50 mg m^{-2}.

492 Using the mean of $N(C_T)$ in NCC and NwAC with the assumption that during the rest of year $N(C_T) = 0$, we

493 calculated the annual $N(C_T)$ of 3.3 mol m^{-2} a^{-1} (Table 3) that its implications are discussed in section 4.3.

494
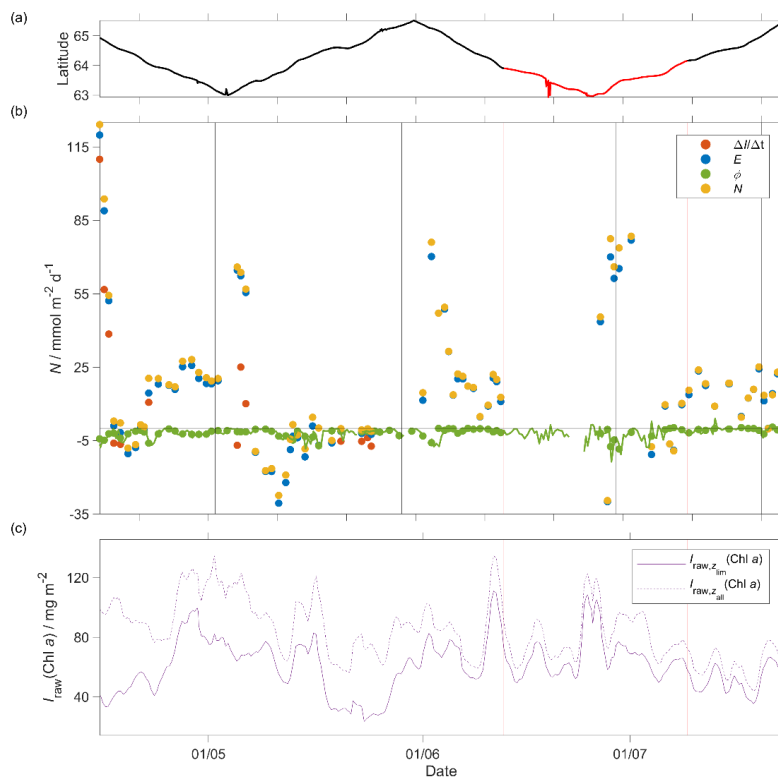
495
496 **Figure 15:** a) shows the trajectory in latitude of the glider where NwAC and NCC are in black and red,

497 respectively. b) Each component of the $N(C_T)$ calculation: in red $\frac{\Delta I(C_T)}{\Delta t}$, $E(C_T)$ in blue, $\Phi(C_T)$ in green dots and

498 the green line is $\Phi(O_2)$ continuous time-series and in yellow $N(C_T) = \frac{\Delta I(C_T)}{\Delta t} + \Phi(C_T)\frac{\min(z_{\text{lim}}, z_{\text{mix}})}{z_{\text{mix}}} - E(C_T)$ c)

499 the violet continuous line is the c_{raw}(Chl a) inventory in the top 45 m, $z_{\text{lim},}$ $(I_{\text{raw},z_{\text{lim}}}$(Chl a)) and the dotted line

500 in all the water columun, $z_{\text{all},}$ $(I_{\text{raw},z_{\text{all}}}$(Chl a)). The black vertical lines represent each glider transect and

501 between the two vertical red lines the glider was in NCC.

502

503 **3.6 Comparison of $N(C_T)$ and $N(O_2)$**

504 To compare $N(C_T)$ and $N(O_2)$, we divided $N(O_2)$ for the photosynthesis quotient (PQ) of 1.9 calculated as the

505 slope of the fitting between $N(C_T)$ and $N(O_2)$ using a geometric mean regression (Leng et al., 2007) excluding

506 the first 2 measurements, designated $N_C(O_2)$. The geometric mean regression was necessary because both the

507 variable had large errors. Figure 16 shows the changes of $N(C_T)$, $N_C(O_2)$ and I_{raw}(Chl a) in time. During the

508 spring and summer periods of increased Chl a inventory, the $N(C_T)$ and $N_C(O_2)$ increased simultaneously.

Ocean Science
Discussions

509   During the spring period of increased Chl a inventory $N(C_T)$ increased to (23 ± 5) mmol m^{-2} d^{-1} and $N(O_2)$ to

510   (32 ± 7) mmol m^{-2} d^{-1}. After the period of increased Chl a inventory, $N(C_T)$ decreased to (-80 ± 107) mmol m^{-2} d^{-1}

511   and $N(O_2)$ to (-7 ± 14) mmol m^{-2} d^{-1}.

512   During the summer period of increased Chl a inventory, $N(C_T)$ and $N(O_2)$ reached the summer maximum in the

513   NwAC region at (75 ± 58) mmol m^{-2} d^{-1} for $N(C_T)$ and (87 ± 39) mmol m^{-2} d^{-1} for $N(O_2)$. Later in the NCC region,

514   the $I_{raw,z_{lim}}$(Chl a) reached a summer maximum of 110 mg m^{-2}, $N(C_T)$ increased to (75 ± 58) mmol m^{-2} d^{-1} and

515    $N(O_2)$ decreased to (-23 ± 66) mmol m^{-2} d^{-1}.

516
517
518
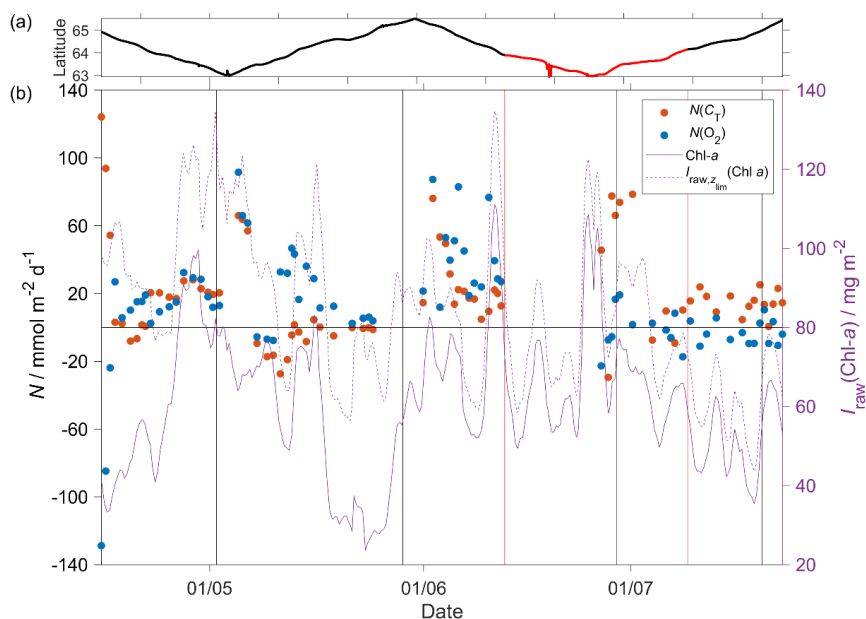
519
520   **Figure 16:** a) shows the trajectory in latitude of the glider where NwAC and NCC are in black and red,
521   respectively. b) Production estimates: in red $N(C)$ and in blue $N(O_2)$ divided per a photosynthesis quotient of
522   1.9. The violet line on the secondary y-axis shows the c_{raw}(Chl a) inventory in the top 45 m, z_{lim},
523    $(I_{raw,z_{lim}}$(Chl a)) and the dotted line in all the water columun, z_{all}, $(I_{raw,z_{all}}$(Chl a)). Also, the black vertical
524   lines represent each glider transect and on the top there is the latitude glider trajectory with NwAC in black and
525   NCC in red.
526

527   **4 Discussion**

528   **4.1 Sensor performance**

529   This study presents data from the first glider deployment with a CO_2 optode. The initial uncalibrated $p(CO_2)$,

530    $p_U(CO_2)$, measured by the CO_2 optode had a median of 604 µatm (5th centile: 566 µatm; 95th centile: 768 µatm

28

531 when the $p(CO_2)$ of discrete samples varied from 302 to 421 µatm. This discrepancy was caused by sensor drift

532 prior to and during deployment of the optode.

533 We applied corrections for drift (using deep-water samples as a reference point), sensor lag and calibrated the

534 CO_2 optode against co-located discrete samples throughout the water column.

535 Atamanchuk (2014) reported that the sensor was affected by a lag that varied from 45 to 264 s depending on

536 temperature. These values were determined in an actively stirred beaker. However, in this study the sensor was

537 mounted on a glider and was not actively pumped, which increased the response time to (1384 s , 25th quartile:

538 1101 s; 75th quartile: 1799 s). Also, the optode was affected by a continuous drift from 637 to 5500 µatm that is

539 larger than the drift found by Atamanchuk et al. (2015a) that increased by 75 µatm after 7 months.

540 In this study, the drift- and lag-corrected sensor output showed a better correlation with the CO_2 concentration

541 $c(CO_2)$ than with $p(CO_2)$. The latter two quantities are related to each other by the solubility that varies with θ

542 and S (Weiss, 1974) (Eq. 2).

543 The calibrated optode output captured the C_T changes in space and time with a standard deviation of 10 µmol

544 kg^{-1} compared with the discrete samples. C_T decreased from 2100 µmol kg^{-1} to 2050 µmol kg^{-1} and increased

545 with depth to 2170 µmol kg^{-1}. This shows the potential of the sensor for future studies that aim to analyse the

546 carbon cycle using a high-resolution dataset.

547 The optode-derived CO_2 fugacity $f_G(CO_2)$ had a mean bias of (8±22) µatm compared with the discrete samples.

548 These values are comparable with a previous study when the CO_2 optode was tested for 65 days on a wave-

549 powered Profiling crAWLER (PRAWLER) from 3 to 80 m (Chu et al., 2020), which had an uncertainty

550 between 35 and 72 µatm. The PRAWLER optode was affected by a continuous drift of 5.5 µatm d^{-1} corrected

551 using a regional empirical algorithm that uses $c(O_2)$, θ, S and σ_o to estimate A_T and C_T.

552 **4.2 Norwegian Sea net community production**

553 Increases in $N(O_2)$ and $N(C_T)$ were associated with increases in depth-integrated c_{raw}(Chl a), designated as

554 periods of increased Chl a inventory, at the beginning of May and in June. During the first period of increased

555 Chl a inventory at the beginning of May surface c_{raw}(Chl a) reached 3 mg m^{-3}. The second period of increased

556 Chl a inventory in June lasted longer and c_{raw}(Chl a) increased to 4 mg m^{-3}. Between the two periods of

557 increased Chl a inventory $N(O_2)$ and $N(C_T)$ had negative values indicating that remineralisation of the high Chl

558 a inventory material was a dominant process during this period. Even though they are uncalibrated, the spring

559 period of increased Chl a inventory c_{raw}(Chl a) values are in agreement with the study of Rey (2001) who found

Ocean Science
Discussions

Open Access

EGU

560   c_{raw}(Chl a) = 3 mg m^{-3} at the beginning of May. The largest period of increased Chl a inventory when the top 50

561   m θ increased from 7 °C to 11 °C and z_{mix} shoaled from 200 m to 20 m. During this period, c(O$_2$) reached a

562   summer maximum of 340 μmol kg^{-1} and C_T decreased to the summer minimum at 2070 μmol kg^{-1}. In both cases,

563   the main components of the N changes were the inventory and air-sea flux, while the smallest driver was the

564   entrainment. Also, the glider sampled two different water masses characterised by different C_T and c(O$_2$). This

565   led to smaller values of N in NCC compared to NwAC.

566   Table 3 shows estimates of net community production (N) in the Norwegian Sea (Falck and Anderson, 2005;

567   Falck and Gade, 1999; Kivimäe, 2007; Skjelvan et al., 2001). All these studies used low-resolution datasets in

568   space and time. These datasets had data collected by several cruises in different years (e. g. 1955 to 1988 (Falck

569   and Gade, 1999)) in all the Norwegian Sea. The estimated N in the 4 studies varies from 2.0 to 8.6 mol m^{-2} a^{-1}

570   for N(C_T) and from 2.6 to 11.1 mol m^{-2} a^{-1} for N(O$_2$). In our study we obtained an annual N in agreement with

571   these studies, with a N(O$_2$) of 10 mol m^{-2} a^{-1} and a N(C_T) of 3.3 mol m^{-2} a^{-1}. The annual N(C_T) and N(O$_2$) that we

572   calculated is most likely an overestimation because it is ignoring the winter and autumn months where N is

573   lower. In fact, for the Nordic Seas Falck and Gade (1999) found a negative N(O$_2$) from October to March.

574   Some of the previous N(C_T) estimates derived C_T from other variables such as c(O$_2$), c(PO$_4^{3-}$), c(NO$_3^-$),

575   assuming Redfield ratios. Our N(C_T) estimate was 3.3 mol m^{-2} a^{-1} and is similar to 3.4 mol m^{-2} a^{-1} estimated by

576   Falck and Anderson (2005) who used C_T samples directly. The difference between our N(C_T) and other studies

577   is likely due to their use of the Redfield ratio assumption (Redfield, 1963) to convert N(O$_2$) to N(C_T). The

578   carbon/nutrients ratios vary between water masses and during photosynthesis (Copin-Montégut, 2000;

579   Körtzinger et al., 2001; Osterroht and Thomas, 2000; Thomas et al., 1999). In deep waters, the release ratios

580   vary for C_T, c(PO$_4^{3-}$), c(NO$_3^-$) and c(O$_2$) leading to different concentrations than the traditional Redfield ratio

581   (Hupe, 2000; Hupe and Karstensen, 2000; Minster and Boulahdid, 1987; Shaffer, 1996). For example, during

582   remineralisation, NO$_3^-$ and PO$_4^{3-}$ are released faster than C_T leading to a C:P remineralisation ratio of 90 ± 15 at

583   the base of the euphotic zone to about 125 ± 10 from to 1000 m to the bottom (Shaffer, 1996).

584   The difference of N(O$_2$) is caused by the yearly variability of N in the Norwegian Sea. In fact, Kivimäe (2007)

585   saw an annual variability of N(O$_2$) from 1955 to 2005 of 4.7 mol m^{-2} a^{-1} to 18.3 mol m^{-2} a^{-1} and of N(C_T) of 3.6

586   mol m^{-2} a^{-1} to 14.0 mol m^{-2} a^{-1}. In order to understand what is causing these interannual changes, it is important

587   to use available high-resolution datasets. Also, this study showed that the Norwegian Sea spring and summer N

588   is strongly affected by time and location. For that reason, N estimated from low-resolution datasets make the

589 result strongly dependant on the time and place of sampling. To quantify this interannual variability in N, more

590 high-resolution studies are needed.

5 Conclusions

592 This study was, to the best of our knowledge, the first glider deployment of a CO_2 optode. During the

593 deployment, the optode performance was affected by drift, lag, lack of sampling in the top 150 m after dive 400

594 (the 24 July 2014), and poor default calibration. We found that the optode response was better correlated with

595 $c(CO_2)$ than $p(CO_2)$. Nevertheless, the optode was able to capture the spatial and temporal changes in the

596 Norwegian Sea after recalibration with discrete samples collected along the glider section and nearby at OWSM

597 during the deployment.

598 C_T estimated from glider data had a standard deviation of 10 μmol kg^{-1} and a mean bias of 1.5 μmol kg^{-1}

599 compared with the discrete samples, while the CO_2 fugacity $f(CO_2)$ had a mean bias of (8±23) μatm. The dataset

600 was used to calculate net community production $N(O_2)$ and $N(C_T)$ from inventory changes, air-sea flux, and

601 entrainment. The two N values had maxima during the summer period of increased Chl a inventory of $N(C_T) =$

602 (64±67) mmol m^{-2} d^{-1} and $N(O_2) =$ (166±75) mmol m^{-2} d^{-1}. At the beginning of April, we sampled a smaller

603 spring period of increased Chl a inventory with a $N(C_T) =$ (23±5) mmol m^{-2} d^{-1} and $N(O_2) =$ (61±14) mmol m^{-2}

604 d^{-1}. After the period of increased Chl a inventory, $N(C_T)$ decreased due to remineralisation to (-80±107) mmol

605 m^{-2} d^{-1}, and $N(O_2)$ to (-15±27) mmol m^{-2} d^{-1}. The glider monitored two water masses (NwAC and NCC). The

606 NCC-influenced one was characterised by a lower $c(O_2)$ and C_T than the NwAC region. $N(O_2)$ decreased to (-

607 43±127) mmol m^{-2} d^{-1} driven by a decrease of $c(O_2)$ under 30 m from 300 to 290 μmol kg^{-1} and increased for

608 $N(C_T)$ to (75±58) mmol m^{-2} d^{-1}. In particular, the $N(O_2)$ changes were driven by the surface oxygen

609 supersaturation making the seawater a source of oxygen. In contrast, the ocean was a sink to inorganic carbon

610 during the summer, with a continuous CO_2 flux from the atmosphere into the water.

611 This deployment shows the potential of using small, low energy consuming CO_2 optodes on autonomous

612 observing platforms like Seagliders to quantify the interactions between biogeochemical processes and the

613 marine carbonate system at high spatiotemporal resolution.

6 References

Alkire, M. B., Lee, C., D'Asaro, E., Perry, M. J., Briggs, N., Cetinić, I. and Gray, A.: Net community production and export from S eaglider measurements in the N orth A tlantic after the spring bloom, J. Geophys. Res. Ocean., 119(9), 6121–6139, 2014.

Atamanchuk, D.: Development and use of an optical pCO2 sensor in marine studies, 2013.

Atamanchuk, D., Tengberg, A., Thomas, P. J., Hovdenes, J., Apostolidis, A., Huber, C. and Hall, P. O. J.: Performance of a lifetime-based optode for measuring partial pressure of carbon dioxide in natural waters, Limnol. Oceanogr. Methods, 12(2), 63–73, doi:10.4319/lom.2014.12.63, 2014.

Atamanchuk, D., Kononets, M., Thomas, P. J., Hovdenes, J., Tengberg, A. and Hall, P. O. J.: Continuous long-term observations of the carbonate system dynamics in the water column of a temperate fjord, J. Mar. Syst., 148, 272–284, doi:10.1016/j.jmarsys.2015.03.002, 2015a.

Atamanchuk, D., Tengberg, A., Aleynik, D., Fietzek, P., Shitashima, K., Lichtschlag, A., Hall, P. O. J. and Stahl, H.: Detection of CO2 leakage from a simulated sub-seabed storage site using three different types of pCO2 sensors, Int. J. Greenh. Gas Control, 38, 121–134, doi:10.1016/j.ijggc.2014.10.021, 2015b.

Bakker, D. C. E., Pfeil, B., Landa, C. S., Metzl, N., Brien, K. M. O., Olsen, A., Smith, K., Cosca, C., Harasawa, S. and Jones, S. D.: A multi-decade record of high-quality f CO 2 data in version 3 of the Surface Ocean CO 2 Atlas (SOCAT), , 383–413, doi:10.5194/essd-8-383-2016, 2016.

Benson, B. B. and Krause Jr, D.: The concentration and isotopic fractionation of oxygen dissolved in freshwater and seawater in equilibrium with the atmosphere 1, Limnol. Oceanogr., 29(3), 620–632, 1984.

Binetti, U., Kaiser, J., Damerell, G. M., Rumyantseva, A., Martin, A. P., Henson, S. and Heywood, K. J.: Net community oxygen production derived from Seaglider deployments at the Porcupine Abyssal Plain site (PAP; northeast Atlantic) in 2012–13, Prog. Oceanogr., 183, 102293, 2020.

Bittig, H. C.: Tackling Oxygen Optode Drift : Near-Surface and In-Air Oxygen Optode Measurements on a Float Provide an Accurate in Situ Reference, , (November), 1536–1543, doi:10.1175/JTECH-D-14-00162.1, 2015.

Bittig, H. C., Fiedler, B., Steinhoff, T. and Körtzinger, A.: OCEANOGRAPHY : METHODS A novel electrochemical calibration setup for oxygen sensors and its use for the stability assessment of Aanderaa optodes, , 1, 921–933, doi:10.4319/lom.2012.10.921, 2012.

von Bültzingslöwen, C., McEvoy, A. K., McDonagh, C., MacCraith, B. D., Klimant, I., Krause, C. and Wolfbeis, O. S.: Sol–gel based optical carbon dioxide sensor employing dual luminophore referencing for application in food packaging technology, Analyst, 127(11), 1478–1483, 2002.

Bushinsky, S. M., Takeshita, Y. and Williams, N. L.: Observing Changes in Ocean Carbonate Chemistry: Our Autonomous Future, Curr. Clim. Chang. reports, 5(3), 207–220, 2019.

Chu, S. N., Sutton, A. J., Alin, S. R., Lawrence-Slavas, N., Atamanchuk, D., Mickett, J. B., Newton, J. A., Meinig, C., Stalin, S. and Tengberg, A.: Field evaluation of a low-powered, profiling p CO2 system in coastal Washington, Limnol. Oceanogr. Methods, n.d.

Copin-Montégut, C.: Consumption and production on scales of a few days of inorganic carbon, nitrate and oxygen by the planktonic community: results of continuous measurements at the Dyfamed Station in the northwestern Mediterranean Sea (May 1995), Deep Sea Res. Part I Oceanogr. Res. Pap., 47(3), 447–477, 2000.

Degrandpre, M. D.: Measurement of Seawater pC02 Using a Renewable-Reagent Fiber Optic Sensor with Colorimetric Detection, , 1172(8), 331–337, doi:10.1021/ac00052a005, 1993.

Dickson, A. G.: Thermodynamics of the dissociation of boric acid in synthetic seawater from 273 . 15 to 318 . 15 K, , 37(5), 755–766, 1990.

Dlugokencky, E. J., Lang, P. M., Masarie, K. A., Crotwell, A. M. and Crotwell, M. J.: Atmospheric carbon dioxide dry air mole fractions from the NOAA ESRL Carbon Cycle Cooperative Global Air Sampling Network, 1968–2014, NOAA ESRL Glob. Monit. Div. Boulder, CO, USA, 2015.

Ducklow, H. W. and Doney, S. C.: What Is the Metabolic State of the Oligotrophic Ocean ? A Debate, , doi:10.1146/annurev-marine-121211-172331, 2013.

Falck, E. and Anderson, L. G.: The dynamics of the carbon cycle in the surface water of the Norwegian Sea, , 94, 43–53, doi:10.1016/j.marchem.2004.08.009, 2005.

Falck, E. and Gade, K.: Net community production and oxygen fluxes in the Nordic Seas based on O2 budget calculations, , 13(4), 1117–1126, 1999.

Fiedler, B., Fietzek, P., Vieira, N., Silva, P., Bittig, H. C. and Körtzinger, A.: In situ CO2 and O2 measurements on a profiling float, J. Atmos. Ocean. Technol., 30(1), 112–126, doi:10.1175/JTECH-D-12-00043.1, 2013.

Foltz, G. R., Grodsky, S. A., Carton, J. A. and McPhaden, M. J.: Seasonal mixed layer heat budget of the tropical Atlantic Ocean, J. Geophys. Res. Ocean., 108(C5), 2003.

Friedlingstein, P., Jones, M., O'Sullivan, M., Andrew, R., Hauck, J., Peters, G., Peters, W., Pongratz, J., Sitch, S. and Le Quéré, C.: Global carbon budget 2019, Earth Syst. Sci. Data, 11(4), 1783–1838, 2019.

Garcia, H. E. and Gordon, L. I.: Oxygen solubility in seawater: Better fitting equations, Limnol. Oceanogr., 37(6), 1307–1312, 1992.

Gattuso, J.-P. and Hansson, L.: Ocean acidification, Oxford University Press., 2011.

Gourcuff, C.: ANFOG Slocum CTD data correction, , (March), 2014.

Ocean Science
Discussions

681   Goyet, C., Walt, D. R. and Brewer, P. G.: Development of a fiber optic sensor for measurement of pCO2 in sea
682   water: design criteria and sea trials, Deep Sea Res. Part A. Oceanogr. Res. Pap., 39(6), 1015–1026, 1992.
683   Hansen, B. and Østerhus, S.: North Atlantic – Nordic Seas exchanges, , 45, 109–208, 2000.
684   Hardman-Mountford, N. J., Moore, G., Bakker, D. C. E., Watson, A. J., Schuster, U., Barciela, R., Hines, A.,
685   Moncoiffé, G., Brown, J., Dye, S., Blackford, J., Somerfield, P. J., Holt, J., Hydes, D. J. and Aiken, J.: An
686   operational monitoring system to provide indicators of CO 2-related variables in the ocean, ICES J. Mar. Sci.,
687   65(8), 1498–1503, doi:10.1093/icesjms/fsn110, 2008.
688   Haskell, W. Z., Hammond, D. E., Prokopenko, M. G., Teel, E. N., Seegers, B. N., Ragan, M. A., Rollins, N. and
689   Jones, B. H.: Net Community Production in a Productive Coastal Ocean From an Autonomous Buoyancy-
690   Driven Glider, J. Geophys. Res. Ocean., 124(6), 4188–4207, 2019.
691   Hemsley, J. M.: OBSERVATIONS PLATFORMS| Buoys, 2015.
692   Hemsley, V. S., Smyth, T. J., Martin, A. P., Frajka-williams, E., Thompson, A. F., Damerell, G. and Painter, S.
693   C.: Estimating Oceanic Primary Production Using Vertical Irradiance and Chlorophyll Pro fi les from Ocean
694   Gliders in the North Atlantic, , doi:10.1021/acs.est.5b00608, 2015.
695   Van Heuven, S., Pierrot, D., Rae, J. W. B., Lewis, E. and Wallace, D. W. R.: MATLAB program developed for
696   CO2 system calculations, ORNL/CDIAC-105b. Carbon Dioxide Inf. Anal. Center, Oak Ridge Natl. Lab. US
697   Dep. Energy, Oak Ridge, Tennessee, 530, 2011.
698   Hupe, A.: Redfield stoichiometry in Arabian Sea subsurface waters, , 14(1), 357–372, 2000.
699   Hupe, A. and Karstensen, J.: Redfield stoichiometry in Arabian Sea subsurface waters, Global Biogeochem.
700   Cycles, 14(1), 357–372, 2000.
701   Jeansson, E., Olsen, A., Eldevik, T., Skjelvan, I., Omar, A. M., Lauvset, S. K., Nilsen, J. E. Ø., Bellerby, R. G.
702   J., Johannessen, T. and Falck, E.: The Nordic Seas carbon budget : Sources , sinks , and uncertainties, ,
703   25(2002), 1–16, doi:10.1029/2010GB003961, 2011.
704   Kara, A. B., Rochford, P. A. and Hurlburt, H. E.: An optimal definition for ocean mixed layer depth, J.
705   Geophys. Res. Ocean., 105(C7), 16803–16821, 2000.
706   Kivimäe, C.: Carbon and oxygen fluxes in the Barents and Norwegian Seas: production, air-sea exchange and
707   budget calculations, 2007.
708   Klimant, I., Huber, C., Liebsch, G., Neurauter, G., Stangelmayer, A. and Wolfbeis, O. S.: Dual lifetime
709   referencing (DLR)—a new scheme for converting fluorescence intensity into a frequency-domain or time-
710   domain information, in New Trends in Fluorescence Spectroscopy, pp. 257–274, Springer., 2001.
711   Körtzinger, A., Thomas, H., Schneider, B., Gronau, N., Mintrop, L. and Duinker, J. C.: At-sea intercomparison
712   of two newly designed underway pCO2 systems—encouraging results, Mar. Chem., 52(2), 133–145, 1996.
713   Körtzinger, A., Koeve, W., Kähler, P. and Mintrop, L.: C: N ratios in the mixed layer during the productive
714   season in the northeast Atlantic Ocean, Deep Sea Res. Part I Oceanogr. Res. Pap., 48(3), 661–688, 2001.
715   Lee, K., Tong, L. T., Millero, F. J., Sabine, C. L., Dickson, A. G., Goyet, C., Park, G. H., Wanninkhof, R.,
716   Feely, R. A. and Key, R. M.: Global relationships of total alkalinity with salinity and temperature in surface
717   waters of the world's oceans, Geophys. Res. Lett., 33(19), 1–5, doi:10.1029/2006GL027207, 2006.
718   Lee, K., Kim, T., Byrne, R. H., Millero, F. J., Feely, R. A. and Liu, Y.: The universal ratio of boron to chlorinity
719   for the North Pacific and North Atlantic oceans, Geochim. Cosmochim. Acta, 74(6), 1801–1811,
720   doi:10.1016/j.gca.2009.12.027, 2010.
721   Leng, L., Zhang, T., Kleinman, L. and Zhu, W.: Ordinary least square regression, orthogonal regression,
722   geometric mean regression and their applications in aerosol science, in Journal of Physics: Conference Series,
723   vol. 78, p. 12084, IOP Publishing., 2007.
724   Lockwood, D., Quay, P. D., Kavanaugh, M. T., Juranek, L. W., Feely, R. A. and À, Æ. C. À.: High-resolution
725   estimates of net community production and air-sea CO 2 flux in the northeast Pacific, , 26, 1–16,
726   doi:10.1029/2012GB004380, 2012.
727   Lueker, T. J., Dickson, A. G. and Keeling, C. D.: Ocean pCO2 calculated from DIC, TA, and the Mehrbach
728   equations for K1 and K2: Validation using laboratory measurements of CO2 in gas and seawater at equilibrium,
729   Abstr. Pap. Am. Chem. Soc., 217, U848–U848, 2000.
730   Martz, T. R., Connery, J. G. and Johnson, K. S.: Testing the Honeywell Durafet for seawater pH applications,
731   Limnol. Oceanogr. Methods, 8, 172–184, doi:10.4319/lom.2010.8.172, 2010.
732   Medeot, N., Nair, R. and Gerin, R.: Laboratory Evaluation and Control of Slocum Glider C – T Sensors, , 838–
733   846, doi:10.1175/2011JTECHO767.1, 2011.
734   Miloshevich, L.: Development and Validation of a Time-Lag Correction for Vaisala Radiosonde Humidity
735   Measurements, , 1305–1328, 2004.
736   Minster, J.-F. and Boulahdid, M.: Redfield ratios along isopycnal surfaces—a complementary study, Deep Sea
737   Res. Part A. Oceanogr. Res. Pap., 34(12), 1981–2003, 1987.
738   Monteiro, P. M. S., Schuster, U., Hood, M., Lenton, A., Metzl, N., Olsen, A., Rogers, K., Sabine, C., Takahashi,
739   T. and Tilbrook, B.: A global sea surface carbon observing system: Assessment of changing sea surface CO2
740   and air-sea CO2 fluxes, Proc. Ocean., 9, 702–714, 2009.
741   Neftel, A., Oeschger, H., Schwander, J., Stauffer, B. and Zumbrunn, R.: Ice core sample measurements give
742   atmospheric CO 2 content during the past 40,000 yr, Nature, 295(5846), 220–223, 1982.

Ocean Science
Discussions

743 Neuer, S., Cianca, A., Helmke, P., Freudenthal, T., Davenport, R., Meggers, H. and Knoll, M.: Progress in
744 Oceanography Biogeochemistry and hydrography in the eastern subtropical North Atlantic gyre . Results from
745 the European time-series station ESTOC, , 72, 1–29, doi:10.1016/j.pocean.2006.08.001, 2007.
746 Nicholson, D., Emerson, S. and Eriksen, C. C.: Net community production in the deep euphotic zone of the
747 subtropical North Pacific gyre from glider surveys, Limnol. Oceanogr., 53(5 PART 2), 2226–2236,
748 doi:10.4319/lo.2008.53.5_part_2.2226, 2008.
749 Nicholson, D. P. and Feen, M. L.: Air calibration of an oxygen optode on an underwater glider, Limnol.
750 Oceanogr. Methods, 15(5), 495–502, doi:10.1002/lom3.10177, 2017.
751 Nilsen, J. E. Ø. and Falck, E.: Progress in Oceanography Variations of mixed layer properties in the Norwegian
752 Sea for the period 1948 – 1999, , 70, 58–90, doi:10.1016/j.pocean.2006.03.014, 2006.
753 Obata, A., Ishizaka, J. and Endoh, M.: Global verification of critical depth theory for phytoplankton bloom with
754 climatological in situ temperature and satellite ocean color data, J. Geophys. Res. Ocean., 101(C9), 20657–
755 20667, 1996.
756 Olsen, A., Key, R. M., Van Heuven, S., Lauvset, S. K., Velo, A., Lin, X., Schirnick, C., Kozyr, A., Tanhua, T.,
757 Hoppema, M., Jutterström, S., Steinfeldt, R., Jeansson, E., Ishii, M., Pérez, F. F. and Suzuki, T.: The global
758 ocean data analysis project version 2 (GLODAPv2) - An internally consistent data product for the world ocean,
759 Earth Syst. Sci. Data, 8(2), 297–323, doi:10.5194/essd-8-297-2016, 2016.
760 Osterroht, C. and Thomas, H.: New production enhanced by nutrient supply from non-Redfield remineralisation
761 of freshly produced organic material, J. Mar. Syst., 25(1), 33–46, 2000.
762 Pachauri, R. K. and Reisinger, A.: IPCC fourth assessment report, IPCC Fourth Assess. Rep., 1, 976 [online]
763 Available from:
764 http://www.construible.es/construible%5Cbiblioteca%5Cpresentacion_informe_ipcc.pdf%5Cnpapers2://publicat
765 ion/uuid/DD3ABB67-E411-4C0F-A29C-DA693B95B789, 2007.
766 Peeters, F., Atamanchuk, D., Tengberg, A., Encinas-Fernández, J. and Hofmann, H.: Lake metabolism:
767 Comparison of lake metabolic rates estimated from a diel CO2-and the common diel O2-technique, PLoS One,
768 11(12), 2016.
769 Plant, J. N., Johnson, K. S., Sakamoto, C. M., Jannasch, H. W., Coletti, L. J., Riser, S. C. and Swift, D. D.: Net
770 community production at Ocean Station Papa observed with nitrate and oxygen sensors on profiling floats,
771 Global Biogeochem. Cycles, 30(6), 859–879, 2016.
772 Quay, P., Stutsman, J. and Steinhoff, T.: Primary production and carbon export rates across the subpolar N.
773 Atlantic Ocean basin based on triple oxygen isotope and dissolved O2 and Ar gas measurements, Global
774 Biogeochem. Cycles, 26(2), 2012.
775 Le Quéré, C., Raupach, M. R., Canadell, J. G., Marland et al., G., Le Quéré et al., C., Le Quéré et al., C.,
776 Raupach, M. R., Canadell, J. G., Marland, G., Bopp, L., Ciais, P., Conway, T. J., Doney, S. C., Feely, R. A.,
777 Foster, P., Friedlingstein, P., Gurney, K., Houghton, R. A., House, J. I., Huntingford, C., Levy, P. E., Lomas, M.
778 R., Majkut, J., Metzl, N., Ometto, J. P., Peters, G. P., Prentice, I. C., Randerson, J. T., Running, S. W.,
779 Sarmiento, J. L., Schuster, U., Sitch, S., Takahashi, T., Viovy, N., van der Werf, G. R. and Woodward, F. I.:
780 Trends in the sources and sinks of carbon dioxide, Nat. Geosci., 2(12), 831–836, doi:10.1038/ngeo689, 2009.
781 Redfield, A. C.: The influence of organisms on the composition of seawater, sea, 2, 26–77, 1963.
782 Rérolle, V. M. C., Floquet, C. F. A., Harris, A. J. K., Mowlem, M. C., Bellerby, R. R. G. J. and Achterberg, E.
783 P.: Development of a colorimetric microfluidic pH sensor for autonomous seawater measurements, Anal. Chim.
784 Acta, 786, 124–131, 2013.
785 Rey, B. F.: 5 . Phytoplankton : the grass of the sea, , (cl), 2001.
786 Sabine, C. L., Feely, R. A., Gruber, N., Key, R. M., Lee, K., Bullister, J. L., Wanninkhof, R., Wong, C. S. S.,
787 Wallace, D. W. R., Tilbrook, B., Millero, F. J., Peng, T.-H. T.-H., Kozyr, A., Ono, T., Rios, A. F., A., F. R.,
788 Gruber, N., Key, R. M., Lee, K., Bullister, J. L., Wanninkhof, R., Wong, C. S. S., Wallace, D. W. R., Tilbrook,
789 B., Millero, F. J., Peng, T.-H. T.-H., Kozyr, A., Ono, T. and Rios, A. F.: The oceanic sink for anthropogenic
790 CO2, Science (80-.)., 305(5682), 367–371, doi:10.1126/science.1097403, 2004.
791 Saderne, V., Fietzek, P. and Herman, P. M. J.: Extreme Variations of pCO2 and pH in a Macrophyte Meadow of
792 the Baltic Sea in Summer: Evidence of the Effect of Photosynthesis and Local Upwelling, PLoS One, 8(4), 2–9,
793 doi:10.1371/journal.pone.0062689, 2013.
794 Saetre, R. and Ljoen, R.: THE NORWEGIAN COASTAL CURRENT, 1972.
795 Seguro, I., Marca, A. D., Painting, S. J., Shutler, J. D., Suggett, D. J. and Kaiser, J.: High-resolution net and
796 gross biological production during a Celtic Sea spring bloom, Prog. Oceanogr., 177, 101885, 2019.
797 Seidel, M. P., Degrandpre, M. D. and Dickson, A. G.: A sensor for in situ indicator-based measurements of
798 seawater pH, , 109, 18–28, doi:10.1016/j.marchem.2007.11.013, 2008.
799 Shaffer, G.: Biogeochemical cycling in the global ocean 2. New production, Redfield ratios, and
800 remineralization in the organic pump, , 101, 3723–3745, 1996.
801 Sharples, J., Ross, O. N., Scott, B. E., Greenstreet, S. P. R. and Fraser, H.: Inter-annual variability in the timing
802 of stratification and the spring bloom in the North-western North Sea, Cont. Shelf Res., 26(6), 733–751, 2006.
803 Skjelvan, I., Falck, E., Anderson, L. G. and Rey, F.: Oxygen fluxes in the Norwegian Atlantic current, Mar.
804 Chem., 73(3–4), 291–303, 2001.

Ocean Science
Discussions

805 Skjelvan, I., Anderson, L. G., Falck, E. and Anders, K.: A Review of the Inorganic Carbon Cycle of the Nordic
806 Seas and Barents Sea and Christoph through the strength area of 15-75, 2005.
807 Skjelvan, I., Falck, E., Rey, F. and Kringstad, S. B.: Inorganic carbon time series at Ocean Weather Station M in
808 the Norwegian Sea, , 549–560, 2008.
809 Sprintall, J. and Roemmich, D.: Characterizing the structure of the surface layer in the Pacific Ocean, J.
810 Geophys. Res. Ocean., 104(C10), 23297–23311, 1999.
811 Sutton, A. J., Sabine, C. L., Meinig, C. and Feely, R. A.: A high-frequency atmospheric and seawater p CO 2
812 data set from 14 open-ocean sites using a moored autonomous system, , 353–366,
813 doi:10.3334/CDIAC/OTG.TSM, 2014.
814 Swift, J. H.: The arctic waters, in The Nordic Seas, pp. 129–154, Springer., 1986.
815 Takahashi, T., Sutherland, S. C., Sweeney, C., Poisson, A., Metzl, N., Tilbrook, B., Bates, N., Wanninkhof, R.,
816 Feely, R. A., Sabine, C., Olafsson, J. and Nojiri, Y.: Global sea – air CO 2 flux based on climatological surface
817 ocean p CO 2 , and seasonal biological and temperature effects, , 49, 1601–1622, 2002.
818 Takahashi, T., Sutherland, S. C., Wanninkhof, R., Sweeney, C., Feely, R. A., Chipman, D. W., Hales, B.,
819 Friederich, G., Chavez, F., Sabine, C., Watson, A., Bakker, D. C. E., Schuster, U., Yoshikawa-Inoue, H., Ishii,
820 M., Midorikawa, T., Nojiri, Y., Körtzinger, A., Steinhoff, T., Hoppema, M., Olafsson, J., Arnarson, T. S.,
821 Johannessen, T., Olsen, A., Bellerby, R., Wong, C. S., Delille, B., Bates, N. R. and de Baar, H. J. W.:
822 Climatological mean and decadal change in surface ocean pCO2, and net sea–air CO2 flux over the global
823 oceans, Deep Sea Res. Part II Top. Stud. Oceanogr., 56(8), 554–577, doi:10.1016/j.dsr2.2008.12.009, 2009.
824 Tengberg, A., Hovdenes, J., Andersson, H. J., Brocandel, O., Diaz, R. and Hebert, D.: OCEANOGRAPHY :
825 METHODS Evaluation of a lifetime-based optode to measure oxygen in aquatic systems, , (1964), 7–17, 2006.
826 Thomas, H., Ittekkot, V., Osterroht, C. and Schneider, B.: Preferential recycling of nutrients—the ocean's way
827 to increase new production and to pass nutrient limitation?, Limnol. Oceanogr., 44(8), 1999–2004, 1999.
828 Thomas, P. J., Atamanchuk, D., Hovdenes, J. and Tengberg, A.: The use of novel optode sensor technologies for
829 monitoring dissolved carbon dioxide and ammonia concentrations under live haul conditions, Aquac. Eng., 77,
830 89–96, 2017.
831 Thompson, R. O. R. Y.: Climatological numerical models of the surface mixed layer of the ocean, J. Phys.
832 Oceanogr., 6(4), 496–503, 1976.
833 United States. National Environmental Satellite and Information Service, D., Monterey, G. I. and Levitus, S.:
834 Seasonal variability of mixed layer depth for the world ocean, US Department of Commerce, National Oceanic
835 and Atmospheric Administration …., 1997.
836 Wanninkhof, R.: OCEANOGRAPHY : METHODS Relationship between wind speed and gas exchange over
837 the ocean revisited, , 351–362, doi:10.4319/lom.2014.12.351, 2014.
838 Weiss, R. F.: Carbon dioxide in water and seawater: the solubility of a non-ideal gas, Mar. Chem., 2(3), 203–
839 215, doi:10.1016/0304-4203(74)90015-2, 1974.
840 Weiss, R. F. and Price, B. A.: Nitrous oxide solubility in water and seawater, Mar. Chem., 8(4), 347–359, 1980.
841 Woolf, D. K. and Thorpe, S. A.: Bubbles and the air-sea exchange of gases in near-saturation conditions, J. Mar.
842 Res., 49(3), 435–466, 1991.
843